The Astrophysical Journal, 836:139 (23pp), 2017 February 10 https://doi.org/10.3847/1538-4357/836/1/139

Multiplicity among Solar-type Stars

K. Fuhrmann[1,2], R. Chini[1,3], L. Kaderhandt[1], and Z. Chen[1,4]
[1] Astronomisches Institut, Ruhr-Universität Bochum, Universitätsstraße 150, D-44801 Bochum, Germany; fuhrmann@astro.rub.de
[2] Isaac Newton Group of Telescopes, Apartado 321, E-38700 Santa Cruz de La Palma, Spain
[3] Instituto de Astronomía, Universidad Católica del Norte, Avenida Angamos 0610, Casilla 1280, Antofagasta, Chile
[4] Purple Mountain Observatory & Key Laboratory for Radio Astronomy, Chinese Academy of Sciences, 2 West Beijing Road, 210008 Nanjing, China
Received 2016 November 14; revised 2017 January 9; accepted 2017 January 9; published 2017 February 14

Abstract

We present a multiplicity census for a volume-complete all-sky survey of 422 stars with distances less than 25 pc and primary main-sequence effective temperatures $T_{\rm eff} \geqslant 5300$ K. Very similar to previous results that have been presented for various subsets of this survey, we confirm the positive correlation of the stellar multiplicities with primary mass. We find for the F- and G-type Population I stars that 58% are non-single and 21% are in triple or higher level systems. For the old intermediate-disk and Population II stars—virtually all of G type and less massive—even two out of three sources prove to be non-single. These numbers being lower limits because of the continuous flow of new discoveries, the unbiased survey clearly demonstrates that the standard case for solar-type field stars is a hydrogen-burning source with at least one ordinary or degenerate stellar companion, and a surprisingly large number of stars are organized in multiple systems. A principal consequence is that orbital evolution, including the formation of blue straggler stars, is a potentially important issue on all spatial scales and timescales for a significant percentage of the stellar systems, in particular among Population II stars. We discuss a number of recent observations of known or suspected companions in the local survey, including a new detection of a double-lined Ba-Bb subsystem to the visual binary HR 8635.

Key words: solar neighborhood – stars: fundamental parameters – stars: solar-type – stars: statistics

1. Introduction

In the context of the formation and evolution of the Galaxy, nearby solar-type stars are prime targets for various reasons. They represent the brightest objects that can still reach back to the early starburst epoch some 12 or 13 Gyr ago. They are mostly slowly rotating sources that are well-suited for spectroscopic investigations at high resolution. The accurate *Hipparcos* astrometry allows for complete local samples that are free of selection biases. With reference to our parent star, model atmosphere analyses and stellar interior calculations both benefit from a direct calibration.

Solar-type stars that are part of spectroscopic binaries are usually less popular in stellar population studies. Although binaries do not need to be a great hurdle for detailed investigations, triple and higher level systems can be made very difficult. Depending on the relative masses and distances of their components, many less well understood evolutionary paths are imaginable for these types of objects, as has been sketched out for instance by Iben & Tutukov (1999) in the context of the important formation of Type Ia supernovae.

In the classical investigations on the multiplicities of solar-type stars by Abt & Levy (1976) and Duquennoy & Mayor (1991), hierarchical systems were underrepresented to a large extent. This happened in part because of observational restrictions at that time, but newly identified companions were also often not inspected in greater detail for the possibility that they might be close subsystems in their own right.

Modern observational techniques and efficient detectors have begun to correct for this bias (e.g., Potter et al. 2002; Pravdo et al. 2006; Ehrenreich et al. 2010; Janson et al. 2012; Jódar et al. 2013; Tokovinin 2013; Chini et al. 2014; Riddle et al. 2015; Rodriguez et al. 2015), and these efforts clearly begin to show that the classical binary successively gives way to more complex hierarchical systems. This is not without positive feedback on the physics of binary stars. The long-standing enigma of the formation of close spectroscopic binaries, for instance, is understood today as a sequel of orbital evolution that is driven by distant companions (cf. Tokovinin et al. 2006).

It is then not only important to know which fraction of solar-type stars is found in binaries, but also how many stars are located in higher level systems and whether this could indeed be a significant number. In their 25 pc all-sky survey of 454 dwarfs with spectral types from about F6 to K3, Raghavan et al. (2010) have advocated a modest 11% fraction for multiple systems, for instance. Their result is, however, subject to selection effects from photometric cutoffs in terms of the relevant primary masses, and, as outlined above, there have been many new discoveries in this field since then.

In our more recent investigations on the multiplicities of local F-type stars (Fuhrmann & Chini 2012, 2015b; hereafter P1 and P2) we find that at least some 25% of these stars consist of triple or higher level systems. In the present work we report that a fraction of 21% is still maintained by inclusion of the local Population I G-type stars. Thus, we learn that a substantial percentage of the Population I solar-type stars is found in systems where orbital evolution is virtually a permanent issue. As opposed to a binary star that mostly depends on nuclear evolution timescales for mass transfer to become important, a third and even distant companion in a higher level system can critically affect the system architecture and both accelerate and terminate the transfer of mass of an inner subsystem.

For the work on stellar populations and the Milky Way evolution mentioned above, a significant fraction of such "uncontrolled" higher level systems represents a major challenge in the sense that very many our field star observations taken at face value can be very misleading.

Derived stellar ages, for instance, may to a large extent depend on unidentified blue straggler stars. As we have already discussed in the accompanying paper (Fuhrmann et al. 2017, hereafter P3), this in fact appears to be the case with the ancient Population II stars, upon which the Galaxy came into being.

It is then clearly of the utmost importance that we can refer to a local census of the stellar multiplicities that is as complete as possible. The steady flow of discoveries (cf. Tokovinin et al. 2015a; Bouchy et al. 2016; Chini et al. 2016; Endl et al. 2016; Fuhrmann et al. 2016; Willmarth et al. 2016; and this work), however, provides not much confidence that this goal could somehow be in reach. Instead, the results on the multiplicities that we present here should be taken as a momentary account, subject to many future updates.

In Section 2 we briefly describe on what kind of observations and analyses this work is based. The set of model atmosphere analyses for almost one hundred stars that complete the all-sky survey is discussed in Section 3. The discussions on the resulting stellar multiplicities are provided in Sections 4 and 5.

2. Observations and Analyses

The spectroscopic data of this work have been collected for a number of years with three different spectrographs. The observations commenced in 1995 September at the Calar Alto Observatory in Spain with the FOCES échelle spectrograph (Pfeiffer et al. 1998) and with a comparatively small 1024^2 CCD, whose 24μ pixel sizes only allowed for a resolution $R = \lambda/\Delta\lambda \simeq 40{,}000$. This configuration was soon upgraded in 1996 October with the introduction of a 2048^2 15μ CCD that resulted in a typical resolution of $R \simeq 60{,}000$. This setup was kept fixed until 2007 August upon completion of the observations at this northern site.

Soon after the project had started at Calar Alto, the *Hipparcos* catalog published a release (Perryman et al. 1997) that for the first time allowed defining a volume-complete sample consisting of F- and G-type stars with distance less than 25 pc. Thus, and in the spirit of early endeavors by Johannes Haas (1930) and Wilhelm Gliese (1957), we began to observe all nearby bright stars with $M_V \leqslant 6.0$ mag, corresponding to eighth magnitude, and at high signal-to-noise ratio (S/N) and high resolution.

From the outset, the specification was to have at least two spectra of each source to assess the reproducibility of the derived stellar parameters from local thermodynamic equilibrium (LTE) model atmosphere analyses. Thereby, redundancy became a major backbone of the project and has proved to be a very valuable concept in the course of the work. A second condition was to have every spectrum exposed to an S/N of at least 200. Early tests with high-resolution spectra secured at S/N $\simeq$ 100 were found to be inadequate for the kind of model atmosphere analyses we aimed at, namely, with accuracies confined to $\Delta T_{\rm eff} \leqslant 80$ K, $\Delta\log g \leqslant 0.10$ dex, and Δ[Fe/H] $\leqslant 0.07$ dex, within 95% (2σ) confidence limits.

The $+37°$ latitude of the Calar Alto Observatory led to a reasonable $\delta = -15°$ southern declination limit for the spectroscopic observations. This limit corresponds to an approximately two-thirds sky coverage and a sample of about 350 stars, more than 90% being solar-type dwarfs. With the $M_V \leqslant 6.0$ mag specification, the faint end of the survey is populated with early-K main-sequence stars, whereas at the bright end there is one B-type star, two dozen A-type stars, and a handful of giants. For reasons explained in the accompanying P3 work on the stellar populations, the lower limit of our survey is defined by a cutoff effective temperature $T_{\rm eff} \geqslant 5300$ K that guarantees an unbiased sample and an essentially complete set of the local F- and G-type stars (cf. Figure 1 in P3).

Upon completion of the analyses of the northern sample (cf. Fuhrmann 2011), observations started in the southern hemisphere in Chile in 2010 April with the BESO échelle spectrograph (Steiner et al. 2006) at the 2800 m altitude Universitätssternwarte Bochum on a side hill of the Cerro Armazones. BESO is basically a clone of the FEROS échelle spectrograph (Kaufer et al. 1999), both producing spectra with an average resolution $R \simeq 50{,}000$ and wavelength coverage $\lambda\lambda 3620 - 8530$ in a single exposure. First results with BESO were presented in Fuhrmann et al. (2011a), followed by two major releases of model atmosphere analyses of southern stars in 2012 and 2015 with P1 and P2. The latter work was in part also based on data secured with FEROS, observations that had begun in 2014 February at the La Silla Observatory in Chile. Here, a main focus was on the search for faint companions to the solar-type stars, such as the M-dwarf spectroscopic binary HR 8635 Ba-Bb reported further below in this work.

As to the survey distance limit, most of the analyses of the northern sample had already been completed when the revised van Leeuwen (2007) *Hipparcos* parallaxes became available. While the southern BESO and FEROS data all took advantage of the improved distance scale, many stars of the northern FOCES sample still require minor updates in that respect. Stars that are no longer within 25 pc on the revised van Leeuwen (2007) scale, however, have now been discarded, and vice versa, few new members been included. For three northern latecomers of this kind, β Aur, HD 45391, and HD 166435, we currently still have no échelle spectra at our disposal, and we rely here on analyses from the literature.

Given the survey size of several hundred sources, there are also a number of visual binaries for which significant progress is still possible with future observations. A prominent example is the classical visual binary γ Vir ($P = 169$ years, $a = 3\farcs6$), a near-equal-mass F-type system at $T_{\rm eff,A} \simeq 6760$ K and $T_{\rm eff,B} \simeq 6730$ K. If not spatially separable, it cannot be resolved spectroscopically because of the considerable projected rotational velocities, $v \sin i_{\rm A} \simeq 36$ km s^{-1} and $v \sin i_{\rm B} \simeq 27$ km s^{-1}, as displayed in Figure 1. In the past 20 years, γ Vir has been a rather difficult system, with its components being closer than 2″ and with the periastron passage at $\rho = 0\farcs37$ in 2005 (cf. Scardia et al. 2007). Because of its $d = 12$ pc nearness and high orbital eccentricity $e = 0.88$, γ Vir will soon start to be clearly separable for at least the next century.

The data reduction of the survey stars includes the usual standard processing, with the resultant spectra being subject to grids of model atmospheres for solar-type dwarfs and subgiants at any metallicity and/or iron-to-α-element abundance mixtures. In brief, the stellar effective temperatures are either derived from the Balmer line wings or refer to the LTE iron ionization equilibrium. The surface gravities mostly rely on the *Hipparcos* astrometry, but also on the prominent Mg Ib triplet lines, as well as on the iron ionization equilibrium. Equivalent widths are measured from theoretical profile fits that include the macroturbulence and projected rotational velocities, as well as the instrumental profile. The microturbulent velocity is set by the usual requirement that the elemental abundances may not depend on the equivalent widths (cf. Fuhrmann et al. 1997).

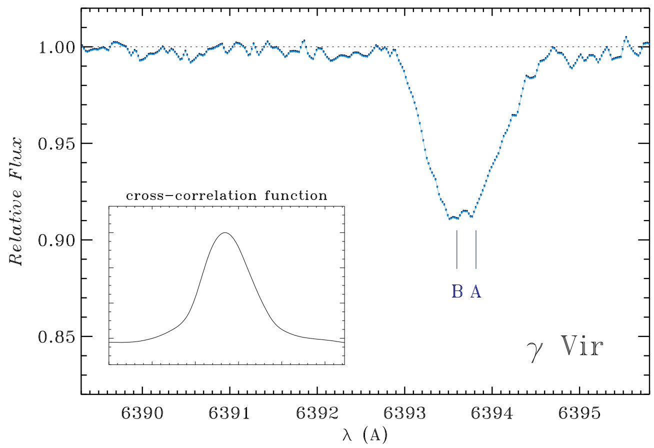

Figure 1. High-resolution, high signal-to-noise ratio spectrum (S/N $\simeq$ 500) of the near-equal-mass F-type visual binary γ Vir (P = 169 years, a = 3$''$.6). The given FOCES spectrum was secured on 2004 February 12, one year before periastron passage, and at maximum Doppler displacement Δv_r(A–B) $\simeq$ +10.2 km s^{-1}. From 1996 until 2014, the components of γ Vir had closed in below 2$''$ angular separation. With projected rotational velocities, $v \sin i_{\rm A} \simeq 36$ km s^{-1} and $v \sin i_{\rm B} \simeq 27$ km s^{-1}, their double-lined spectrum remains unresolved. Because of its d = 12 pc nearness and a high orbital eccentricity e = 0.88, γ Vir will soon again be clearly separable for at least the next century. The inset shows the cross-correlation function; the asymmetric profile is caused by the different projected rotational velocities.

With the final set of model atmosphere analyses for this survey, we again present several observations and reanalyses of stars that have been part of our previous work, mostly that of P1 and P2. These analyses basically serve to verify the results of previous campaigns to ensure redundancy and reproducibility toward a set of basic stellar parameters as homogeneous as possible.

3. The Southern Stars

As with the previous analyses of this survey, the derived stellar parameters for single or single-lined stars are set out in Table 1, unless some interesting circumstances deserve a special mention. The uncertainties in Table 1 are all meant as 2σ errors, although, and rather conservatively, we prefer to adopt fixed values of 0.1 dex, 0.2 km s^{-1}, 0.05 dex, and 0.05 mag for the surface gravity $\log g$, microturbulence ξ_t, abundance ratio [Fe/Mg], and bolometric correction BC_V, respectively. Note that in this section we also include four analyses/reanalyses of the northern sample stars γ Cet, ψ^1 Dra, HD 218687, and ι Psc.

With respect to the FEROS radial velocities of faint common-proper-motion sources or candidates with $V < 15$ mag, we adopt the Population II star 82 Eri as the velocity standard with $v_r = +87.953$ km s^{-1} (Pepe et al. 2011). Repeated observations of other G dwarfs assumed to be single, such as the Population II star ν^2 Lup, then lead to rms uncertainties down to 0.027 km s^{-1}, whereas the rms uncertainties for the much fainter M-dwarf companions are assessed as <0.5 km s^{-1}. Compared to the radial velocities of Nordström et al. (2004) for 54 slowly rotating and presumably single solar-type stars in common with our sample, we derive a zero-point offset $\Delta v_r = +0.38$ km s^{-1}, whereas for the subset of 10 stars in common with the work of Nidever et al. (2002), we use essentially the same velocity scale at $\Delta v_r = +0.03$ km s^{-1}.

θ Scl = HD 739. In Table 2 we present two sets of radial velocities (2015 July and December) for this single-lined spectroscopic binary with rms uncertainties of 0.05 km s^{-1}. As it turns out, both sets cover similar orbital phases, which means that the period is only constrained to $P \simeq 179/n$ day, with $n \leqslant 14$. A plausible $n = 4$ case ($P \simeq 44.6$ days), along with three radial velocities from Andersen & Nordström (1983), is illustrated in Figure 2.

HD 870. As the kinematics $U/V/W = +19/+13/+6$ km s^{-1} suggests, HD 870 may belong to the Ursa Major Association. Although the chromospheric activity (Hα, Ca II H&K) is reduced, this is not unexpected, as this loose grouping of young stars does not necessarily need to have the same age. We note, however, that HD 870 shares the same iron abundance and the characteristic barium overabundance of that association.

HD 1237. The kinematics ($U/V/W = -23/-11/+10$ km s^{-1}), iron abundance ([Fe/H] = +0.10), coronal (Hünsch et al. 1999) and chromospheric (Naef et al. 2001) activity of HD 1237 all support a Hyades stream membership, as has been pointed out by Naef et al. (2001).

HD 1273. This is a $P = 411$ day spectroscopic (Bopp et al. 1970) and astrometric (Catchpole 1972; Jancart et al. 2005) binary, whose secondary we identify in Figure 3 as a red dwarf. This single-epoch spectrum, secured on 2015 June 30 at orbital phase $\Phi \simeq 0.83$, shows the Aa and Ab components partly separated at $\Delta v_r = +10.5$ km s^{-1}. Both components being main-sequence stars, an iterative, composite spectrum synthesis leads to a $\Delta m_V \simeq 3.7$ mag fainter secondary with an effective temperature $T_{\rm eff,Ab} \simeq 4030$ K, whereas the composite Balmer line wings result in $T_{\rm eff,Aa} \simeq 5735$ K for the primary. With $\log g_{\rm Aa} \simeq 4.46$ and $\log g_{\rm Ab} \simeq 4.79$ from the *Hipparcos* parallax, the composite modeling of HD 1273 Aa–Ab—as in Figure 3 with the Fe I line λ6246.326 and Fe II line λ6247.564—shows that HD 1273 is a fairly metal-poor Population I star at [Fe/H] $\simeq -0.50$ and [Fe/Mg] $\simeq -0.15$. With reference to the VandenBerg et al. (2006) evolutionary tracks, the stellar masses are $M_{\rm Aa} \simeq 0.86\,M_\odot$ and $M_{\rm Ab} \simeq 0.53\,M_\odot$. For the individual stellar magnitudes, radii, and the rotational velocity of the primary, we obtain $V_{\rm Aa} \simeq 6.86$, $M_{V,\rm Aa} \simeq 5.09$, $M_{\rm bol,Aa} \simeq 4.93$, $R_{\rm Aa} \simeq 0.91\,R_\odot$, $v \sin i_{\rm Aa} \simeq 1.5$ km s^{-1}, and $V_{\rm Ab} \simeq 10.56$, $M_{V,\rm Ab} \simeq 8.80$, $M_{\rm bol,Ab} \simeq 7.82$, and $R_{\rm Ab} \simeq 0.49\,R_\odot$.

With the radial velocities, $v_{r,\rm Aa} = -17.67$ km s^{-1} and $v_{r,\rm Ab} = -7.26$ km s^{-1}, derived from the composite spectrum synthesis, and the above stellar masses, the systemic velocity is obtained as $\gamma = -13.70 \pm 0.20$ km s^{-1}.

HR 176 = HD 3823. A discussion of this star has recently been presented in Chini et al. (2016). It is included in Table 1 for completeness reasons.

HR 209 = HD 4391. Our 2015 July and December radial velocities for this wide ($\rho_{\rm A-B} = 17''$, $\rho_{\rm A-C} = 47''$) triple system are summarized in Table 3; the small differences are fully compatible with orbital motion. As displayed in Figure 4, all three components are chromospherically active, which also demonstrates their physical association.

HD 4747. Its space velocity and weak chromospheric activity suggest that HD 4747 might be a Hyades stream member (e.g., Eggen 1960, 1996). This is difficult to reconcile with the low iron abundance [Fe/H] = −0.25, however. If it is not related to the Hyades, the question remains what causes the observed level of chromospheric activity. The low-mass companion with a minimum orbital period of about 20 years (Nidever et al. 2002; Sahlmann et al. 2011) is no source in the

Table 1
Stellar Parameters of the Final Set of Single or Single-lined Program Stars

Object	HR	HD	V (mag)	$T_{\rm eff}$ (K)	log g (cgs)	[Fe/H] (dex)	ξ_t (km s^{-1})	[Fe/Mg] (dex)	$\zeta_{\rm RT}$ (km s^{-1})	$v \sin i$ (km s^{-1})	$M_{\rm bol}$ (mag)	BC_V (mag)	Mass ($M_\odot$)	Radius ($R_\odot$)
θ Scl Aa[a]	35	739	5.236	6394	4.24	−0.09	1.55	−0.03	5.7	1.0	3.52	−0.08	1.25	1.40
			0.005	80	0.10	0.07	0.20	0.05		1.0	0.05	0.05		0.05
		870	7.227	5353	4.57	−0.08	0.77	+0.00	1.9	2.6	5.48	−0.22	0.89	0.81
			0.005	80	0.10	0.07	0.20	0.05		1.0	0.06	0.05		0.03
		1237 A	6.584	5475	4.53	+0.10	1.05	+0.04	2.4	5.3	5.18	−0.19	0.98	0.89
			0.005	70	0.10	0.06	0.20	0.05		0.6	0.05	0.05		0.03
	176 A	3823	5.894	5967	4.15	−0.30	1.22	−0.13	4.3	1.5	3.78	−0.12	1.05	1.42
			0.005	60	0.10	0.06	0.20	0.05		1.0	0.05	0.05		0.05
		4308	6.544	5683	4.36	−0.35	0.99	−0.32	3.2	1.0	4.66	−0.16	0.92	1.05
			0.005	70	0.10	0.07	0.20	0.05		1.0	0.05	0.05		0.04
	209 A[b]	4391	5.791	5807	4.47	−0.11	0.95	−0.03	3.7	2.9	4.75	−0.13	1.00	0.96
			0.005	60	0.10	0.06	0.20	0.05		0.6	0.05	0.05		0.03
		4747 A	7.157	5337	4.58	−0.25	0.85	−0.07	1.8	2.3	5.57	−0.23	0.85	0.78
			0.005	80	0.10	0.07	0.20	0.05		1.0	0.05	0.05		0.03
ν Phe[a]	370	7570	4.966	6066	4.31	+0.16	1.15	+0.01	4.7	3.7	3.98	−0.09	1.17	1.26
			0.005	70	0.10	0.06	0.20	0.05		0.5	0.05	0.05		0.04
κ Tuc B	377	7788	7.633	5145	4.63	+0.15	1.06	+0.03	1.1	4.4	5.81[c]	−0.29	0.88	0.75
			0.030	90	0.10	0.07	0.20	0.05		0.8	0.07	0.05		0.04
		9540	6.972	5429	4.57	−0.03	0.84	+0.01	2.2	2.0	5.37	−0.20	0.93	0.83
			0.005	70	0.10	0.06	0.20	0.05		1.0	0.05	0.05		0.03
	506	10647	5.518	6069	4.37	−0.08	1.16	+0.01	4.7	5.0	4.21	−0.10	1.09	1.13
			0.005	70	0.10	0.06	0.20	0.05		0.6	0.05	0.05		0.04
	683	14412	6.333	5394	4.59	−0.49	0.77	−0.14	2.1	2.0	5.60	−0.22	0.82	0.76
			0.005	70	0.10	0.06	0.20	0.05		1.0	0.05	0.05		0.03
ι Hor[a]	810	17051	5.399	6057	4.37	+0.15	1.13	+0.03	4.7	5.7	4.14	−0.09	1.16	1.17
			0.005	60	0.10	0.06	0.20	0.05		0.6	0.05	0.05		0.04
		20407	6.753	5853	4.42	−0.46	1.10	−0.18	3.8	1.0	4.69	−0.15	0.92	0.98
			0.005	60	0.10	0.07	0.20	0.05		1.0	0.05	0.05		0.03
ζ^1 Ret[b]	1006	20766	5.506	5726	4.51	−0.24	0.95	−0.11	3.4	2.2	4.96	−0.15	0.95	0.90
			0.005	60	0.10	0.06	0.20	0.05		0.8	0.05	0.05		0.03
ζ^2 Ret[b]	1010	20807	5.226	5838	4.44	−0.25	0.98	−0.11	3.8	1.5	4.69	−0.14	0.96	0.98
			0.005	60	0.10	0.06	0.20	0.05		1.0	0.05	0.05		0.03
		21175 A	6.915	5245	4.56	+0.18	0.79	+0.02	1.5	2.5	5.47[c]	−0.25	0.95	0.85
			0.005	70	0.10	0.06	0.20	0.05		1.0	0.06	0.05		0.03
κ Ret A[a]	1083	22001	4.705	6554	4.10	−0.17	1.91	−0.06	7.0	14.3	2.95	−0.07	1.37	1.73
			0.005	80	0.10	0.07	0.20	0.05		0.6	0.05	0.05		0.06
		23484	6.995	5161	4.59	+0.12	0.82	+0.05	1.1	3.1	5.69	−0.28	0.89	0.79
			0.005	80	0.10	0.07	0.20	0.05		0.7	0.05	0.05		0.03
τ^6 Eri[a]	1173	23754	4.214	6496	4.09	+0.03	1.75	−0.07	6.7	14.7	2.92	−0.06	1.43	1.78
			0.005	80	0.10	0.06	0.20	0.05		0.6	0.05	0.05		0.06
58 Eri	1532	30495	5.488	5801	4.49	−0.01	1.06	+0.00	3.7	3.1	4.74	−0.13	1.05	0.97
			0.005	70	0.10	0.06	0.20	0.05		0.8	0.05	0.05		0.03
		30501 A	7.585	5119	4.56	−0.01	0.85	−0.01	1.0	2.6	5.69	−0.30	0.85	0.80
			0.005	80	0.10	0.07	0.20	0.05		1.0	0.05	0.05		0.03
		32778 Aa	7.019	5684	4.50	−0.59	0.94	−0.19	3.0	1.0	5.08	−0.18	0.85	0.86
			0.005	60	0.10	0.06	0.20	0.05		1.0	0.05	0.05		0.03
	1747	34721	5.954	5961	4.19	−0.10	1.20	−0.07	4.7	2.3	3.85	−0.11	1.07	1.38
			0.005	70	0.10	0.07	0.20	0.05		0.8	0.05	0.05		0.05
γ Lep A[a]	1983	38393	3.585	6255	4.27	−0.08	1.28	−0.05	5.5	8.0	3.75	−0.08	1.18	1.32
			0.005	70	0.10	0.06	0.20	0.05		0.5	0.05	0.05		0.04
π Men	2022	39091	5.662	5924	4.33	+0.04	1.13	+0.02	4.5	1.5	4.24	−0.11	1.07	1.17
			0.005	60	0.10	0.06	0.20	0.05		1.0	0.05	0.05		0.04
		53143[b]	6.818	5408	4.55	+0.12	1.04	+0.02	2.1	4.8	5.30	−0.21	0.96	0.86

Table 1
(Continued)

Object	HR	HD	V (mag)	$T_{\rm eff}$ (K)	log g (cgs)	[Fe/H] (dex)	ξ_t (km s^{-1})	[Fe/Mg] (dex)	$\zeta_{\rm RT}$ (km s^{-1})	$v \sin i$ (km s^{-1})	$M_{\rm bol}$ (mag)	BC_V (mag)	Mass ($M_\odot$)	Radius ($R_\odot$)
			0.015	70	0.10	0.06	0.20	0.05		0.6	0.05	0.05		0.03
	2667	53705	5.568	5812	4.28	−0.22	1.07	−0.18	3.7	1.0	4.29	−0.14	0.98	1.19
			0.032	60	0.10	0.06	0.20	0.05		1.0	0.07	0.05		0.04
	2668	53706	6.905	5298	4.55	−0.22	0.79	−0.17	1.7	1.8	5.52	−0.24	0.85	0.81
			0.091	70	0.10	0.06	0.20	0.05		1.0	0.11	0.05		0.05
		59468[b]	6.721	5601	4.40	+0.03	0.87	−0.03	2.9	1.8	4.78	−0.16	0.96	1.02
			0.005	70	0.10	0.06	0.20	0.05		1.0	0.05	0.05		0.04
	2882[b]	59967	6.656	5787	4.50	−0.08	1.04	+0.00	3.6	3.7	4.83	−0.14	1.02	0.94
			0.005	60	0.10	0.06	0.20	0.05		0.6	0.05	0.05		0.03
	3570[a]	76653	5.699	6311	4.29	+0.00	1.57	−0.03	5.7	10.6	3.71	−0.08	1.23	1.32
			0.005	80	0.10	0.07	0.20	0.05		0.5	0.05	0.05		0.05
	3862[a]	84117	4.923	6102	4.28	−0.07	1.18	−0.03	4.9	5.1	3.94	−0.10	1.12	1.27
			0.005	70	0.10	0.06	0.20	0.05		0.6	0.05	0.05		0.04
	4134 A[a]	91324	4.885	6127	3.97	−0.27	1.33	−0.12	5.5	8.8	3.09	−0.11	1.18	1.86
			0.005	70	0.10	0.06	0.20	0.05		0.6	0.05	0.05		0.06
	4979[a]	114613	4.847	5682	3.89	+0.14	1.12	+0.00	4.2	1.7	3.13	−0.14	1.27	2.12
			0.005	60	0.10	0.06	0.20	0.05		1.0	0.05	0.05		0.07
		120559 Aa	7.967	5513	4.51	−0.97	1.03	−0.44	2.4	1.0	5.73[d]	−0.21	0.71	0.68
			0.005	70	0.10	0.07	0.20	0.05		1.0	0.07	0.05		0.03
	5356 A[a]	125276	5.855	6052	4.38	−0.65	1.19	−0.18	4.6	1.0	4.43	−0.14	0.93	1.03
			0.005	60	0.10	0.06	0.20	0.05		1.0	0.06	0.05		0.04
	5632	134060	6.296	5863	4.31	+0.06	1.04	+0.00	3.9	2.0	4.26	−0.12	1.05	1.18
			0.005	70	0.10	0.07	0.20	0.05		1.0	0.06	0.05		0.04
		145825 A	6.550	5792	4.48	+0.03	0.97	+0.00	3.6	1.5	4.75	−0.13	1.04	0.97
			0.005	60	0.10	0.06	0.20	0.05		1.0	0.06	0.05		0.03
ζ TrA Aa[a]	6098	147584	4.898	6032	4.43	−0.09	1.19	−0.01	4.5	1.0	4.38	−0.11	1.09	1.06
			0.005	70	0.10	0.06	0.20	0.05		1.0	0.05	0.05		0.04
		154088	6.585	5379	4.52	+0.38	0.80	+0.04	2.0	2.0	5.12	−0.21	1.07	0.95
			0.005	80	0.10	0.07	0.20	0.05		1.0	0.05	0.05		0.04
ξ Oph A[a]	6445	156897	4.373	6611	4.15	−0.27	2.06	−0.08	7.2	20.2	3.10	−0.08	1.30	1.59
			0.005	80	0.10	0.07	0.20	0.05		0.7	0.05	0.05		0.06
μ Ara[a]	6585	160691	5.125	5725	4.22	+0.28	1.01	+0.02	3.9	2.0	4.04	−0.13	1.13	1.37
			0.005	60	0.10	0.06	0.20	0.05		1.0	0.05	0.05		0.04
ψ^1 Dra B[f]	6637	162004	5.752	6188	4.27	−0.03	1.24	−0.04	5.2	5.4	3.85	−0.09	1.16	1.28
			0.010	70	0.10	0.06	0.20	0.05		0.7	0.06	0.05		0.05
	6748 A	165185	5.936	5895	4.46	−0.09	1.04	+0.01	4.0	7.6	4.59	−0.12	1.06	1.01
			0.005	60	0.10	0.07	0.20	0.05		0.5	0.05	0.05		0.03
ι Pav Aa[a]	6761	165499	5.468	5901	4.26	−0.10	1.09	−0.05	4.1	2.0	4.12	−0.12	1.03	1.25
			0.005	70	0.10	0.06	0.20	0.05		1.0	0.05	0.05		0.04
	6828 A	167425	6.170	6016	4.39	+0.10	1.26	+0.02	4.5	2.5	4.26	−0.10	1.13	1.12
			0.005	70	0.10	0.07	0.20	0.05		1.0	0.05	0.05		0.04
	7232	177565	6.154	5624	4.44	+0.08	0.89	+0.00	3.0	1.5	4.85	−0.16	0.96	0.98
			0.005	60	0.10	0.06	0.20	0.05		1.0	0.05	0.05		0.03
	7330 Aa	181321	6.484	5792	4.50	−0.08	1.00	+0.02	3.6	12.4	4.82[e]	−0.13	1.01	0.94
			0.005	70	0.10	0.07	0.20	0.05		0.7	0.28	0.05		0.13
	7644	189567	6.070	5727	4.38	−0.28	1.00	−0.13	3.4	1.0	4.67	−0.15	0.93	1.03
			0.005	70	0.10	0.07	0.20	0.05		1.0	0.05	0.05		0.04
δ Pav[a]	7665	190248	3.550	5621	4.35	+0.36	0.94	+0.03	3.0	2.0	4.47	−0.15	1.12	1.17
			0.005	70	0.10	0.07	0.20	0.05		1.0	0.05	0.05		0.04
	7674	190422	6.256	6084	4.43	−0.09	1.28	−0.02	4.8	15.3	4.31	−0.10	1.14	1.08
			0.005	80	0.10	0.07	0.20	0.05		0.5	0.06	0.05		0.04
	7722	192310	5.733	5072	4.53	+0.09	0.55	+0.01	0.8	2.3	5.67	−0.32	0.85	0.83

Table 1
(Continued)

Object	HR	HD	V (mag)	$T_{\rm eff}$ (K)	log g (cgs)	[Fe/H] (dex)	ξ_t (km s^{-1})	[Fe/Mg] (dex)	$\zeta_{\rm RT}$ (km s^{-1})	$v \sin i$ (km s^{-1})	$M_{\rm bol}$ (mag)	BC_V (mag)	Mass ($M_\odot$)	Radius ($R_\odot$)
			0.005	80	0.10	0.07	0.20	0.05		1.0	0.05	0.05		0.03
		194640	6.619	5526	4.45	−0.03	0.78	−0.02	2.6	1.5	4.99	−0.18	0.90	0.95
			0.005	70	0.10	0.07	0.20	0.05		1.0	0.06	0.05		0.04
ϕ^2Pav[a]	7875	196378	5.109	6012	3.91	−0.42	1.42	−0.18	5.2	5.4	3.02	−0.13	1.17	1.99
			0.005	80	0.10	0.06	0.20	0.05		0.6	0.05	0.05		0.07
	7898	196761	6.364	5457	4.55	−0.30	0.81	−0.10	2.3	1.5	5.37	−0.20	0.87	0.82
			0.005	80	0.10	0.07	0.20	0.05		1.0	0.05	0.05		0.03
		197214 Aa	6.953	5632	4.48	−0.26	0.89	−0.08	3.0	1.0	5.04	−0.17	0.88	0.90
			0.005	60	0.10	0.06	0.20	0.05		1.0	0.07	0.05		0.03
	8013	199260	5.699	6188	4.29	−0.14	1.18	−0.03	5.2	13.9	3.90	−0.09	1.12	1.26
			0.005	80	0.10	0.07	0.20	0.05		0.5	0.05	0.05		0.05
		199288	6.512	5815	4.35	−0.70	1.17	−0.37	3.5	1.0	4.62	−0.16	0.85	1.02
			0.005	70	0.10	0.07	0.20	0.05		1.0	0.05	0.05		0.04
		199509 A	6.985	5781	4.50	−0.37	0.97	−0.13	3.4	1.0	4.95	−0.15	0.91	0.89
			0.005	70	0.10	0.07	0.20	0.05		1.0	0.05	0.05		0.03
		202628	6.747	5798	4.44	−0.04	0.99	−0.01	3.7	2.3	4.68	−0.13	1.00	1.00
			0.005	70	0.10	0.07	0.20	0.05		1.0	0.06	0.05		0.04
		203244 Aa	6.982	5565	4.55	−0.14	0.94	−0.01	2.7	3.7	5.26	−0.18	0.94	0.83
			0.005	70	0.10	0.07	0.20	0.05		0.7	0.06	0.05		0.03
		203985 Aa	7.488	5203	4.55	+0.36	0.80	+0.00	1.3	2.5	5.37	−0.27	1.01	0.90
			0.005	80	0.10	0.07	0.20	0.05		1.0	0.08	0.05		0.05
		205536	7.065	5446	4.47	−0.03	0.83	−0.07	2.3	2.0	5.15	−0.20	0.89	0.91
			0.005	80	0.10	0.07	0.20	0.05		1.0	0.06	0.05		0.04
	8477[b]	210918	6.220	5748	4.28	−0.13	0.98	−0.10	3.6	1.0	4.36	−0.14	0.97	1.18
			0.005	70	0.10	0.06	0.20	0.05		1.0	0.05	0.05		0.04
	8501 A	211415	5.370	5846	4.38	−0.25	1.06	−0.10	3.8	1.5	4.54	−0.14	0.97	1.05
			0.005	60	0.10	0.06	0.20	0.05		1.0	0.05	0.05		0.03
	8526 A	212168	6.116	5887	4.29	+0.00	1.04	−0.04	4.2	2.0	4.19	−0.12	1.05	1.22
			0.015	70	0.10	0.06	0.20	0.05		1.0	0.06	0.05		0.04
	8635 A	214953	5.981	6047	4.30	+0.04	1.20	−0.01	4.6	3.4	4.02	−0.10	1.13	1.25
			0.005	70	0.10	0.06	0.20	0.05		0.6	0.05	0.05		0.04
		218687 Aa[f]	6.541	5887	4.37	−0.14	1.33	−0.04	4.1	10.0	4.44	−0.13	1.00	1.08
			0.005	70	0.10	0.07	0.20	0.05		0.7	0.06	0.05		0.04
		222335	7.185	5219	4.55	−0.17	0.69	−0.02	1.4	2.2	5.58	−0.26	0.86	0.82
			0.005	80	0.10	0.07	0.20	0.05		0.8	0.06	0.05		0.03
ι Psc[f]	8969	222368	4.123	6164	4.07	−0.16	1.41	−0.10	5.6	5.2	3.34	−0.10	1.17	1.64
			0.005	70	0.10	0.06	0.20	0.05		0.7	0.05	0.05		0.05

Notes. For each star the second row gives 2σ error estimates, with the errors of log g, ξ_t, [Fe/Mg], and BC_V generally assessed as 0.1 dex, 0.2 km s^{-1}, 0.05 dex, and 0.05 mag, respectively. Macroturbulent velocities $\zeta_{\rm RT}$ are adopted from the relations in Gray (1984, 1992). The bolometric corrections are taken from Alonso et al. (1995). Uncertainties in the stellar masses are likely lower than 10%.

[a] Reanalysis of P1.

[b] Reanalysis of P2.

[c] The given value refers to the Söderhjelm (1999) parallax.

[d] The given value refers to the *Hipparcos* parallax, the spectroscopic parallax would instead result in $M_{\rm bol,Aa} = 5.44$.

[e] The given value refers to the spectroscopic parallax.

[f] Northern sample star.

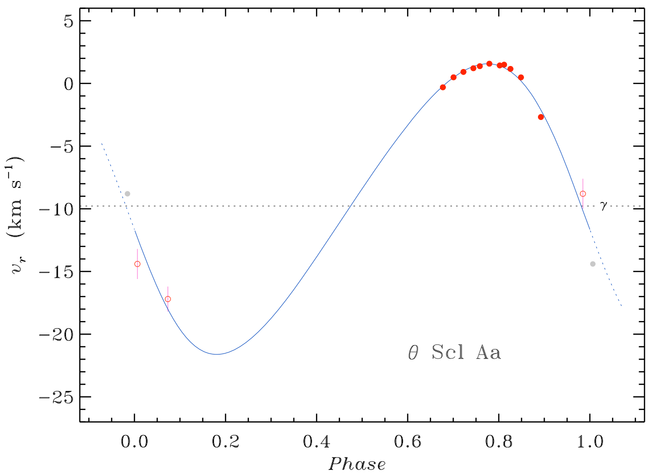

Figure 2. Velocity curve for θ Scl Aa assuming $P \simeq 44.6$ days. Error bars denote 2σ uncertainties. Open circles are three radial velocities from Andersen & Nordström (1983). Note that on the basis of these velocities, the given curve illustrates only a plausible case (see text for details).

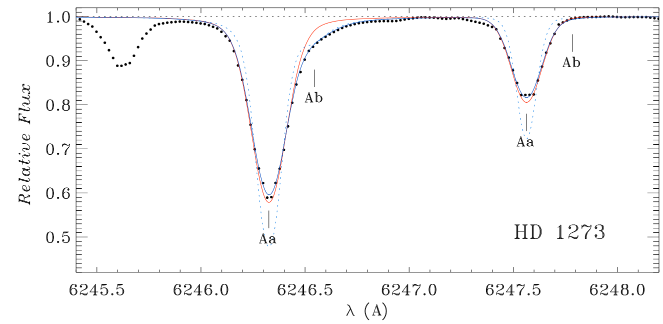

Figure 3. Modeling of the Fe I line λ6246.326 and Fe II line λ6247.564 for the $P = 411$ day double-lined spectroscopic binary HD 1273. Both components, separated here at $\Delta v_r = +10.5$ km s^{-1}, are main-sequence stars with $\Delta m_V \simeq 3.7$ mag at effective temperatures $T_{\rm eff,Aa} \simeq 5735$ K and $T_{\rm eff,Ab} \simeq 4030$ K. HD 1273 is also a metal-poor star at [Fe/H] $\simeq -0.50$. The light blue dotted curve denotes the synthetic composite spectrum before instrumental convolution. The dark blue curve accounts for the secondary, whereas it is excluded with the red curve. Note that HD 1273 Ab is directly visible in the red wing of the strong Fe I line, but note also its impact by filling in the Fe II line of HD 1273 Aa. The corresponding effect on the abundance amounts to Δ[Fe/H] $\simeq +0.05$ dex.

Table 2
Radial Velocity Measurements of θ Scl Aa

MJD	Aa (km s^{-1})	MJD	Aa (km s^{-1})
57203.4223	+1.38	57378.0866	−0.31
57204.3575	+1.57	57379.1282	+0.49
57205.3754	+1.44	57380.0959	+0.92
57206.4273	+1.16	57381.0685	+1.21
57207.4525	+0.48	57384.0776	+1.50
57209.4000	−2.68	⋯	⋯

Table 3
Radial Velocity Measurements of the Wide Triple HR 209

MJD	A (km s^{-1})	B (km s^{-1})	C (km s^{-1})
57206.4	−10.67	−11.24	⋯
57380.1	−10.46	−11.24	⋯
57381.1	−10.56	⋯	−11.69

first place, but its impact for a secular orbital evolution and the accretion of a third component on HD 4747 A cannot be excluded.

κ Tuc = HD 7693/7788. This is a prominent southern hierarchical quadruple system in a stable 2 + 2 configuration. The pair with the bright F-type primary is HR 377 = HD 7788 AB, whose K-type secondary is currently separated at $\rho \simeq 4\farcs5$ in a $P = 857$ year orbit (Scardia & Pansecchi 2005). The 5′ distant, fainter pair is HD 7693 AB and consists of two K-type stars in a $P = 85$ year orbit (Heintz 1978; Söderhjelm 1999).

A model atmosphere analysis of the F-type primary HD 7788 A faces the difficulty of a considerable projected rotational velocity $v \sin i_{\rm A} = 60$ km s^{-1}. From the Balmer line wings we obtain an effective temperature $T_{\rm eff,A} = 6474$ K, and, with reference to the $\pi = 49.4 \pm 0.9$ mas Söderhjelm (1999) parallax of HD 7693, a surface gravity $\log g_{\rm A} = 4.24$. For a determination of the iron abundance, there are no suitable Fe II lines and the Fe I lines are known to produce LTE abundances that are systematically too low by Δ[Fe/H] $\simeq -0.15$ dex in this part of the H-R diagram (cf. Steffen 1985; Fuhrmann et al. 1997). In this situation, we assume consistent iron abundances for HD 7788 A and B, which for the latter we derive as [Fe/H] = +0.15 (cf. Table 1), in agreement with its Hyades stream membership. With this metallicity and with reference to $V_{\rm A} = 4.941$, $M_{V,\rm A} = 3.41$, and $M_{\rm bol,A} = 3.36$, we derive a primary mass $M_{\rm A} \simeq 1.36\,M_\odot$ and a stellar radius $R_{\rm A} = 1.47\,R_\odot$. From our single-epoch FEROS spectra of HD 7788 A and B we measure the following radial velocities: $v_{r,\rm A} = +9.38$ km s^{-1} and $v_{r,\rm B} = +8.25$ km s^{-1} on 2015 December 22, and $v_{r,\rm A} = +9.40$ km s^{-1} on 2015 December 24.

HD 9540. Kinematically, this star is in the vicinity of the Hercules–Lyra Association. With a comparatively weak chromospheric activity for Ca II H&K and Hα, however, it may not be younger than 1 Gyr.

For the $\rho = 5.6'$ distant late-K main-sequence star Gl 59 B = NLTT 5160, we measure a radial velocity $v_r = -3.25$ km s^{-1}, compared to $v_r = +2.59$ km s^{-1} for HD 9540 (= Gl 59 A). NLTT 5160 shows no evidence of being chromospherically active, and for reasonable effective temperatures in the range $T_{\rm eff} = 4000$–4300 K, we derive spectroscopic distances of 66–96 pc, which confirms the conclusion by Raghavan et al. (2010) that NLTT 5160 is an unrelated optical companion.

HD 9770. The distant and faint M-dwarf companion to this K-type star was discovered in 1881 by S.W. Burnham at $\rho = 1\farcs8$. As pointed out by Eggen (1952), "The pair became of special interest when B. Dawson, in 1920, found the brighter star to be double, with two nearly equal components of very small separation." The semimajor axis $a = 0\farcs17$ and orbital period $P = 4.56$ year that were later derived by Dawson (1933) are also the modern values (Tokovinin et al. 2015a). It still took several decades and space-borne observations in the ultraviolet and X-rays (Pounds et al. 1993; Bowyer et al. 1994) to realize that because of the extreme brightness of the AB-C triple at these wavelengths, some information of key importance was still lacking.

Intense photometric monitoring soon hereafter showed that the B component is itself a very close eclipsing binary at

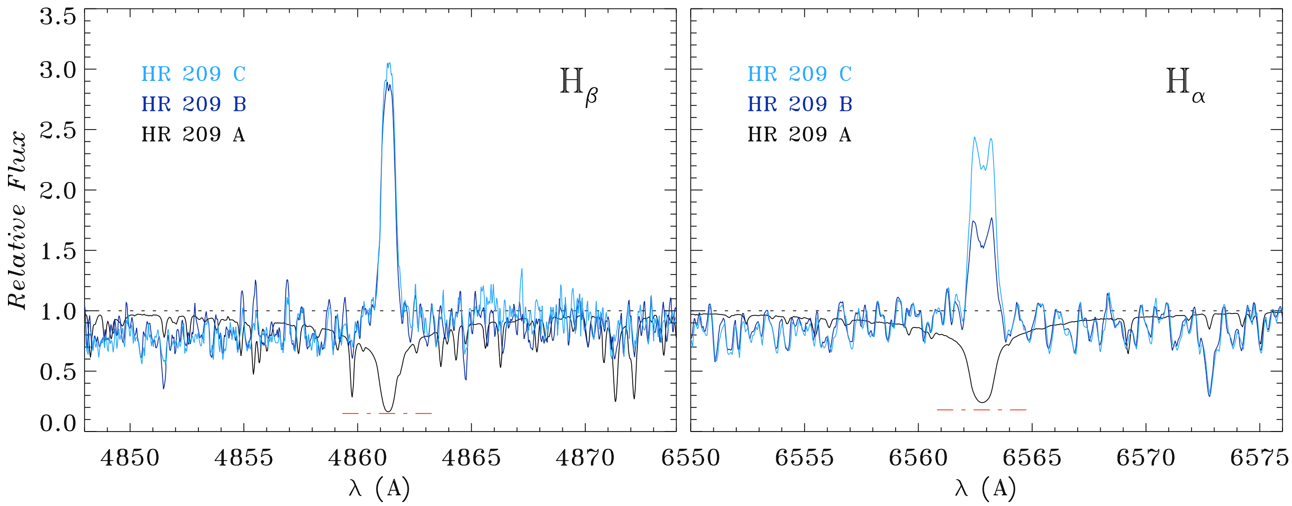

Figure 4. High-resolution spectra of the A, B, and C components of HR 209 in the vicinity of the Hβ (left) and Hα (right) lines. HR 209 A is a relatively young chromospherically active G-type star with a slightly filled-in Hα line core. (The red dash–dotted lines in both panels provide fiducial marks for inactive G stars.) HR 209 B and HR 209 C, in turn, are faint M dwarfs that show their Balmer lines in emission. Along with the common radial velocities in Table 3, this demonstrates their physical association with the primary.

$P = 0.48$ days (Cutispoto et al. 1995, 1997; Bromage et al. 1996; Tagliaferri et al. 1999). Its photometry and eclipses show that the Ba-Bb subcomponents are both K-type stars in an essentially circular orbit, but the relative photometry of A versus B remains a major uncertainty. In particular, Watson et al. (2001) have demonstrated from the eclipse photometry that the individual *Hipparcos* H_p magnitudes are erroneous.

In what follows, we adopt the relative photometry of Watson et al. (2001), and for the absolute magnitudes we make use of the Söderhjelm (1999) $\pi = 46.42 \pm 1.10$ mas parallax. For the distant M dwarf ($P = 123$ years, Hartkopf & Mason 2010), which at the epoch of our observations (2015 December) was separated at $\rho \simeq 1''\!.6$, we may assume a negligible contribution on our spectra. In Figure 5 we show a portion of the triple-lined spectrum of HD 9770 around the Fe I lines λ6056.010 and λ6065.493, along with a composite modeling. As it turns out, and at variance with what has repeatedly been stated in the literature, HD 9770 is not a metal-poor star, but has a close-to-solar iron abundance. Ignoring the Ba and Bb components, the slowly rotating rather inactive primary would purport an abundance [Fe/H] ~ -0.80, beyond the local Population I limit (cf. Figure 3 in P3); and in contradiction to its kinematics. The broad $v \sin i \sim 83$ km s^{-1} Ba and Bb contributions, separated at $\Delta v_{r,\mathrm{Ba}} \sim +132$ km s^{-1} to the red and $\Delta v_{r,\mathrm{Bb}} \sim -138$ km s^{-1} to the blue of HD 9770 A in Figure 5, however, necessarily lead to a weakening of the primary lines, and, if accounted for, an essentially solar metallicity. In view of the uncertain photometry mentioned above, and with the general difficulty of a precise modeling of a very broadened and active binary like HD 9770 Ba-Bb, we can only present provisional stellar parameters: $T_{\mathrm{eff,A}} \simeq 5210$ K, $T_{\mathrm{eff,Ba}} \simeq 4600$ K, and $T_{\mathrm{eff,Bb}} \simeq 4460$ K for the effective temperatures, and $M_{\mathrm{A}} \simeq 0.88\,M_\odot$, $M_{\mathrm{Ba}} \simeq 0.74\,M_\odot$, and $M_{\mathrm{Bb}} \simeq 0.71\,M_\odot$ for the stellar masses.

HR 683 = HD 14412. The Ca II H&K and Hα lines show a weak chromospheric activity. The kinematics and the unevolved main-sequence stage, however, provide no clue whether this is a signature of youth or accretion.

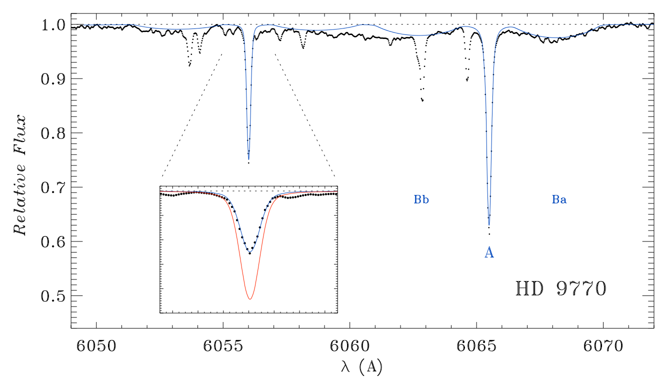

Figure 5. Modeling of the Fe I lines λ6056.010 and λ6065.493 for the triple-lined HD 9770 system. The A, Ba, and Bb components are all K dwarfs with inner and outer orbital periods of $P = 0.48$ day (Ba-Bb) and $P = 4.56$ years (A-B). While the HD 9770 A primary is a slowly rotating source at $v \sin i_{\mathrm{A}} \simeq 2.5$ km s^{-1}, the Ba and Bb companions are in bound rotation with projected rotational velocities $v \sin i \sim 83$ km s^{-1}, separated here at $\Delta v_{r,\mathrm{Ba}} \sim +132$ km s^{-1} and $\Delta v_{r,\mathrm{Bb}} \sim -138$ km s^{-1} with respect to HD 9770 A. The blue curve is the synthetic modeling of the three components at $T_{\mathrm{eff,A}} \simeq 5210$ K, $T_{\mathrm{eff,Ba}} \simeq 4600$ K, $T_{\mathrm{eff,Bb}} \simeq 4460$ K, and [Fe/H] = +0.04. The inset highlights the HD 9770 A λ6056 Fe I line with (blue) or without (red) the contribution of the Ba-Bb subsystem.

γ Cet = HD 16970. For this latecomer of the northern sample from the revised van Leeuwen (2007) *Hipparcos* parallax, we briefly discuss two spectra, one centered on the A-type primary, and one centered on the F-type secondary, which is displaced by 2″ and is three magnitudes fainter. Although the A-type primary falls beyond our grid of model atmospheres, and although our spectrum of the secondary is strongly impacted by this bright A star, there are several points that can be readily deduced for the secondary. In the first place, and with the constraint of an implausible position below the main sequence, γ Cet B must be as cool as $T_{\mathrm{eff,B}} \sim 6000$ K, with a $\log g_{\mathrm{B}} \sim 4.46$ from its bolometric magnitude $M_{\mathrm{bol,B}} = 4.55$. We also find that γ Cet B has a projected rotational velocity $v \sin i_{\mathrm{B}} \sim 10$ km s^{-1}, a strong lithium λ6707 resonance line, and a strong barium overabundance.

In combination with the kinematics, $U/V/W = +31/+3/-5\,\mathrm{km\,s^{-1}}$, this supports an Ursa Major Association membership (Mohr 1930) and suggests that γ Cet B is very similar to the early-G star HR 1322 of this association. For the radial velocities we measure $v_{r,\mathrm{A}} = -1.12\,\mathrm{km\,s^{-1}}$ and $v_{r,\mathrm{B}} = -10.68\,\mathrm{km\,s^{-1}}$. With mass estimates of $M_\mathrm{A} \simeq 2.00\,M_\odot$ and $M_\mathrm{B} \simeq 1.10\,M_\odot$, this provides a systemic velocity $\gamma = -4.5\,\mathrm{km\,s^{-1}}$.

HD 21175. For this visual binary ($P = 238$ years), the $\rho \simeq 2\farcs6$ distant and $\Delta m_I \simeq 3$ mag (Tokovinin et al. 2015a) fainter secondary is not visible in our 2015 December spectra of HD 21175 A. The K-type primary shows a weak chromospheric activity, compared to the $L_x = 105.3 \times 10^{27}$ erg s^{-1} (Hünsch et al. 1999) X-ray luminosity, which may be a hint for a short-period Ba-Bb subsystem.

κ Ret = HD 22001. A single FEROS spectrum of the M-dwarf secondary provides no evidence for a Ba-Bb spectroscopic subsystem. Our radial velocities of this wide binary are as follows: $v_{r,\mathrm{A}} = +13.59\,\mathrm{km\,s^{-1}}$ and $v_{r,\mathrm{B}} = +15.61\,\mathrm{km\,s^{-1}}$ (2015 December 24), and $v_{r,\mathrm{A}} = +13.49\,\mathrm{km\,s^{-1}}$ (2015 December 28).

HD 23484. The kinematics, chromospheric activity, and iron abundance consistently confirm that HD 23484 must be a Hyades stream member.

HR 1294 = HD 26491. The preliminary analysis of the HR 1294 A G-type primary leads to an old Population I turnoff star with an effective temperature $T_{\mathrm{eff,A}} \simeq 5786$ K, surface gravity $\log g_\mathrm{A} \simeq 4.27$, metallicities [Fe/H] $\simeq -0.13$ and [Fe/Mg] $\simeq -0.05$, and mass $M_\mathrm{A} \simeq 0.97\,M_\odot$, which all depend to some extent on the contribution of the HR 1294 B secondary.

Jenkins et al. (2015) recently presented a first provisional $P = 26.7$ year spectroscopic orbit with a $M_\mathrm{B} = 0.50 \pm 0.15\,M_\odot$ minimum mass. From their radial velocity curve we can estimate that a three to five magnitudes fainter K- or M-dwarf companion should be redshifted by less than $\Delta v_r \sim 4\,\mathrm{km\,s^{-1}}$ in our 2015 December epoch spectra, which is too small to be detectable from line profile asymmetries. On the other hand, and given the fairly long orbital period, any brighter K-dwarf companion should have been visible to *Hipparcos*, as it should also be visible from the wings of strong lines, e.g., the Mg Ib triplet, which is not the case. Even a $\Delta m_V = 4$ mag fainter red dwarf would be present in the spectra by filling in the Balmer line wings of its primary, however, such that the above $T_{\mathrm{eff,A}} \simeq 5786$ K would be revised to $T_{\mathrm{eff,A}} \simeq 5820$ K. The radial velocity curve of Jenkins et al. (2015) implies that the next years will lead to Doppler separations $\Delta v_r \geqslant +10\,\mathrm{km\,s^{-1}}$, which should clarify the role of the secondary.

58 Eri = HD 30495. The coronal (Hünsch et al. 1999) and chromospheric activity both suggest this to be a young star. In view of its kinematics, $U/V/W = -14/-3/+4\,\mathrm{km\,s^{-1}}$, 58 Eri might be related to the IC 2391 cluster.

HD 30501. With its kinematics, $U/V/W = +48/+5/-40\,\mathrm{km\,s^{-1}}$, this source does not reside in a region in velocity space usually occupied by nearby young stars (cf. Figure 10 in P3). The fact that the K-type HD 30501 A primary is chromospherically active (Hα, Ca II H&K, $v \sin i$) may therefore rather be related to an orbital evolution and mass transfer, possibly driven by the HD 30501 B secondary in its $P = 2073.6$ day (Sahlmann et al. 2011) eccentric orbit.

HD 32778. Two aspects of this old Population I star deserve a brief mention: first, the *Hipparcos* photometry shows a huge $\Delta H_p = 0.4$ mag amplitude for the HD 32778 Aa primary, which cannot be intrinsic to this chromospherically inactive G dwarf. On the other hand, Jenkins et al. (2010) provisionally estimated an orbital period of 6.5 years for the Aa–Ab subsystem, with HD 32778 Ab being a brown dwarf candidate, such that even a perfectly aligned eclipsing system would not cause the observed photometric variation.

Table 4
Hipparcos Astrometry and Photometry of the Multiple System HR 2667/8 and HD 53680

HR	HD	System component	π (mas)	H_p (mag)
2667	53705	A	60.55 ± 1.04	5.7033 ± 0.0320
2668	53706	B	47.99 ± 9.89	7.0459 ± 0.0909
	53680	Cab	57.42 ± 1.16	8.8041 ± 0.0017
	...	$\langle\pi\rangle$	59.09 ± 0.77	...

For the $\rho \simeq 80''$ distant red dwarf companion, HD 32778 B, and second, we obtain an effective temperature $T_{\mathrm{eff,B}} \simeq 4040$ K, a stellar mass $M_\mathrm{B} \simeq 0.53\,M_\odot$, and a consistent radial velocity $v_{r,\mathrm{B}} = +2.68\,\mathrm{km\,s^{-1}}$ from our single-epoch spectrum (2015 December). We find no compelling evidence for a Ba-Bb subsystem, but note that the Ca II H&K lines of HD 32778 B are in emission.

HR 1747 = HD 34721. With the revised van Leeuwen (2007) *Hipparcos* parallax, $\pi = 39.96 \pm 0.40$ mas, this star is no longer part of the local 25 pc sample.

π Men = HD 39091. For this 5–6 Gyr old high-velocity turnoff star, Jones et al. (2002) have pointed out in their discovery paper that the massive extra-solar planet candidate they had found "may plausibly be a brown dwarf." Their attempt to constrain the companion mass with the *Hipparcos* intermediate astrometric data at that time remained inconclusive. The more recent work by Reffert & Quirrenbach (2011) on the basis of the revised van Leeuwen (2007) *Hipparcos* data indeed appears to favor a brown dwarf mass. We note in this context that the low projected rotational velocity, $v \sin i = 1.5 \pm 1.0\,\mathrm{km\,s^{-1}}$, that we measure is only in keeping with a fairly old chromospherically inactive G-type star and not suited to solve the issue. For the time being, we keep π Men as a binary candidate.

HR 2667/8 = HD 53705/6. This visual pair, consisting of a G-type turnoff star (HR 2667) and an early-K dwarf secondary (HR 2668), displays a chemistry intermediate to that of Population I and II (cf. Figure 3 in P3). This implies an old system with an age of about 10 Gyr (cf. Bernkopf & Fuhrmann 2006). The $3'$ distant K6V common-proper-motion companion, HD 53680, is itself an astrometric and spectroscopic binary. For its primary we estimate $T_{\mathrm{eff,Ca}} \simeq 4390$ K and $M_\mathrm{Ca} \simeq 0.69\,M_\odot$,[5] assuming the same metallicity and age as for HR 2667/8. A preliminary orbital solution of the HD 53680 Ca-Cb subsystem was given by Makarov et al. (2008), who found an orbital period of about 4 years and a $M_\mathrm{Cb} \simeq 0.2\,M_\odot$ low-mass secondary; similar values were later derived by Sahlmann et al. (2011) for a combined astrometric/spectroscopic orbit.

Table 4 shows that there are considerable uncertainties with the *Hipparcos* astrometry and photometry of this multiple

[5] Most of the stellar parameters of HD 53680 in Table 2 of Sahlmann et al. (2011) must be mistaken.

system. The parallax that we adopt, $\pi = 59.09 \pm 0.77$ mas, is a weighted mean.

HR 2882 = HD 59967. This star has been briefly discussed in P2 and is again mentioned further below in connection with HR 7330 and 53 Aqr and the young "Octans-Near Association" (Zuckerman et al. 2013).

In 2015 December we additionally took a single 1 hr FEROS exposure of the faint source 2MASS J07303984-3720233 at $\rho = 32''$. According to the exposure, this is a distant unrelated giant at $v_r = +106.42$ km s^{-1}, compared to $v_r = +9.50$ km s^{-1} for HR 2882.

HR 3570 = HD 76653. To the discussion of this star in P1, we add that its low [Ba/Fe]$= -0.05$ abundance ratio is not compatible with an Ursa Major Association membership. This also implies that HR 3570 is probably not a very wide companion of δ Vel, as suggested by Shaya & Olling (2011). With a nominal age of around 2 Gyr we repeat our previous concern that it is difficult to reconcile this age with the high X-ray luminosity $L_x = 214.3 \times 10^{27}$ erg s^{-1} (Hünsch et al. 1999), which might rather point to a more recent accretion event.

HD 120559. This old Population II star is frequently used as a local calibrator to the distance scale and the ages of globular clusters (e.g., Chaboyer et al. 1998; Carretta et al. 2000; Grundahl et al. 2002; Percival et al. 2002; Bergbusch & Stetson 2009; VandenBerg et al. 2010). The work by Raghavan et al. (2010) lists HD 120559 as a single star, ignoring the radial velocity variation of several km s^{-1} found by Nordström et al. (2004), which we do confirm from our FEROS spectra secured on 2014 February 10 ($v_r = +12.81$ km s^{-1}), 2015 June 30 ($v_r = +15.26$ km s^{-1}), and 2015 July 2 ($v_r = +15.34$ km s^{-1}), all three velocities with an rms uncertainty of 0.03 km s^{-1}.

With a *Hipparcos* parallax $\pi = 40.02 \pm 1.00$ mas, HD 120559 was originally part of our 25 pc sample, but its parallax has more recently been revised to $\pi = 39.42 \pm 0.97$ mas (van Leeuwen 2007). In both *Hipparcos* astrometric solutions the invisible Ab component has not been taken into account, however, and our model atmosphere analysis indeed implies an even greater distance of about 29 pc. If true, the absolute bolometric magnitude of the G-type primary would be $M_{\rm bol,Aa} = 5.44$ instead of $M_{\rm bol,Aa} = 5.73$ (cf. Table 1), with a potentially important bearing on the calibrations of globular cluster distances and ages described above.[6]

HR 5209 = HD 120690. For this astrometric, spectroscopic, and visual binary with a 10.5 year period (Abt & Willmarth 2006; Tokovinin 2012; Jenkins et al. 2015; Willmarth et al. 2016), spectroscopically resolved observations are only possible for a small part of its eccentric orbit, the next window being around the year 2020. Of the two échelle spectra currently at our disposal, the first was secured on 2014 February 12; it is photometrically unbiased, but displays only a weak $\Delta v_r \simeq -7$ km s^{-1} Doppler separation. The second spectrum, secured on 2015 July 3, is much better resolved at $\Delta v_r = -11.3$ km s^{-1}; it is also characterized by a loss of light of the secondary at the fiber entrance due to an increased $\rho \simeq 0\overset{''}{.}3$ angular separation by that epoch. For a quantitative analysis this can easily be accounted for, however, as long as the velocity offset of the secondary is sufficiently large and its spectral contribution directly visible. Accordingly, we concentrate here on this 2015 epoch spectrum.

Otherwise, our analysis proceeds in essentially the same manner as described above for HD 1273, except that we can directly refer to the visual magnitudes $V_{\rm A} = 6.48$ and $V_{\rm B} = 9.87$ from Tokovinin (2014a) based on speckle interferometric measurements. In particular, we get very much the same diagnostics as in Figure 3: symmetric Fe II line profiles, compared to asymmetries for the Fe I lines, this time blueshifted at $\Delta v_r = -11.3$ km s^{-1}, however. Assuming solar abundances (as approximately confirmed below), the visual magnitude for the secondary leads to a main-sequence position $T_{\rm eff,B} \simeq 4070$ K, and from the composite Balmer line wings a primary effective temperature $T_{\rm eff,A} \simeq 5680$ K follows. The surface gravities, $\log g_{\rm A} \simeq 4.49$ and $\log g_{\rm B} \simeq 4.72$ from the *Hipparcos* parallax suggest an unevolved main-sequence primary, in line with the spectroscopic iron ionization equilibrium. With abundances [Fe/H] $\simeq +0.05$ and [Fe/Mg] $\simeq -0.03$, evolutionary tracks provide a rather young $\tau \sim 2$ Gyr star with component masses $M_{\rm A} \simeq 1.01\,M_\odot$ and $M_{\rm B} \simeq 0.62\,M_\odot$. The other relevant stellar parameters are $M_{V,\rm A} = 5.04$, $M_{\rm bol,A} = 4.89$, $R_{\rm A} \simeq 0.95\,R_\odot$, $v \sin i_{\rm A} \simeq 2.0$ km s^{-1}, and $M_{V,\rm B} \simeq 8.43$, $M_{\rm bol,B} \simeq 7.43$, and $R_{\rm B} \simeq 0.57\,R_\odot$.

HR 5356 = HD 125276. The results of the reanalysis of the F-type primary of this visual binary are presented in Table 1. The secondary, displayed by the FEROS guiding camera at approximately $\theta \simeq 235°$ and $\rho \simeq 4\overset{''}{.}1$ on 2015 July 1, was too close and too faint for an individual exposure, however. The radial velocity trend very recently reported by Borgniet et al. (2016) is likely caused by this companion.

HD 130042. Although this star has been discovered as a visual binary in 1929 (Donner 1953), this is a less studied southern Population I object with an orbital period $P = 261$ years (Zirm 2014). At the epoch of our spectroscopic observations (2015 July), the $\Delta m_V = 2.2$ mag fainter secondary was separated at $\rho \simeq 2\overset{''}{.}3$ (Tokovinin et al. 2014), meaning that a significant part of its light also passed the $2''$ entrance aperture of the spectrograph while the primary was observed. As a result, the secondary affects the Balmer line effective temperature determination (by filling in the line wings of its primary), as well as the surface gravity determination if based on the iron ionization equilibrium. The cross-correlation function does not reveal an asymmetry, however, which implies that the radial velocity of the B component cannot have been much different, and hence, the overall iron abundance is not much affected.

A composite modeling of the A and B components of HD 130042 confirms that the velocity offset amounts to only 2 km s^{-1}. The effect of the secondary on the Balmer line wings is approximately assessed as 40 K. Instead of $T_{\rm eff,A} = 5342$ K that is derived by ignoring the secondary, we obtain $T_{\rm eff,A} \simeq 5380$ K in the composite analysis. The surface gravity is hereafter fixed from the *Hipparcos* parallax to $\log g_{\rm A} \simeq 4.47$, and from the iron and magnesium abundances, [Fe/H] $\simeq +0.07$ and [Fe/Mg] $\simeq +0.02$, evolutionary tracks lead to stellar masses $M_{\rm A} \simeq 0.89\,M_\odot$ and $M_{\rm B} \simeq 0.69\,M_\odot$. As an unevolved main-sequence star, the late-K secondary is here placed at $T_{\rm eff,B} \simeq 4360$ K and $\log g_{\rm B} \simeq 4.66$. We also point out the bolometric magnitudes and stellar radii, which result in $M_{\rm bol,A} \simeq 5.20$, $R_{\rm A} \simeq 0.91\ R_\odot$ and $M_{\rm bol,B} \simeq 6.87$, $R_{\rm B} \simeq 0.65\ R_\odot$ for HD 130042 A and B, respectively.

[6] The very recent *Gaia* DR1 release leads to a parallax $\pi = 29.77 \pm 0.76$ mas. Although this should be subject to future revisions from the astrometric orbit, it appears save to conclude that HD 120559 is very unlikely a 25 pc sample member.

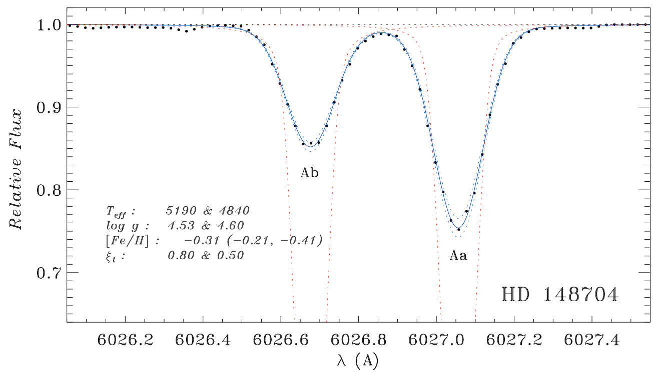

Figure 6. Modeling of the Fe I line λ6027.056 in the composite spectrum of the $P = 31.8$ day spectroscopic binary HD 148704. Stellar parameters for the spectrum synthesis (dark blue) are as given in the legend. The light blue dotted curves denote abundance changes of Δ[Fe/H] $= \pm0.10$ dex. Individual line profiles for the slowly rotating $v\sin i_{\rm Aa} \simeq v\sin i_{\rm Ab} \simeq 1.5\ {\rm km\ s^{-1}}$, Δv_r Aa − Ab $= +18.9\ {\rm km\ s^{-1}}$ (2015 July 1) Doppler-displaced components are given by the red dotted curves.

HD 148704. This is a spectroscopic binary with an orbital period $P = 31.8$ days (Bopp et al. 1970), consisting of two early-K dwarfs. A tenth-magnitude background star unfortunately passed the line of sight to HD 148704 in the last two decades (cf. Raghavan et al. 2010; Tokovinin et al. 2015b), and this is the cause for the fairly uncertain *Hipparcos* parallax, $\pi = 40.77 \pm 2.01$ mas (van Leeuwen 2007).

Although, as it turns out, HD 148704 is not part of our local sample, for its Aa primary falls short of our cut-off effective temperature of $T_{\rm eff} \geqslant 5300$ K, we briefly discuss the basic stellar parameters of this binary. To this end, and in view of the parallax uncertainty and the short orbital period, we note that we do not have a precise absolute magnitude of HD 148704, nor do we know the relative photometry of its components. The basic constraints that we can refer to are the Balmer line wings for an effective temperature determination and the relative strength of the resolved absorption lines from high-resolution spectra as displayed in Figure 6 with the Fe I line λ6027.056. With the additional information of a fairly hot kinematics, $U/V/W = -58/-39/+12\ {\rm km\ s^{-1}}$, and the chromospheric and coronal inactivity (Hünsch et al. 1999), we can further assume an old Population I member status for HD 148704, i.e., both its components must be unevolved main-sequence stars.

From these constraints, we infer the secondary to be $\Delta m_V \simeq 0.7$ mag fainter at $T_{\rm eff,Ab} \simeq 4840$ K and $\log g_{\rm Ab} \simeq 4.60$, and $T_{\rm eff,Aa} \simeq 5190$ K and $\log g_{\rm Aa} \simeq 4.53$ for the primary. The composite modeling shows that as in Figure 6, HD 148704 is a slightly metal-poor star at [Fe/H] $\simeq -0.33$ and [Fe/Mg] $\simeq -0.13$, which, with reference to evolutionary tracks, leads to main-sequence stellar masses $M_{\rm Aa} \simeq 0.79\,M_\odot$ and $M_{\rm Ab} \simeq 0.72\,M_\odot$.

With these stellar masses, the two epochs of radial velocities that we can refer to, $v_{r,\rm Aa} = -41.68\ {\rm km\ s^{-1}}$ and $v_{r,\rm Ab} = -60.58\ {\rm km\ s^{-1}}$ (2015 July 1), and $v_{r,\rm Aa} = -60.68\ {\rm km\ s^{-1}}$ and $v_{r,\rm Ab} = -39.83\ {\rm km\ s^{-1}}$ (2015 July 4), result in a systemic velocity $\gamma = -50.71 \pm 0.20\ {\rm km\ s^{-1}}$, in very good agreement with the original Bopp et al. (1970) value $\gamma = -50.59 \pm 0.20\ {\rm km\ s^{-1}}$. For the G-type optical companion 2MASS J16313011-3900383, now at an angular distance of about 10″ northeast of HD 148704, we derive $v_{r,\rm opt} = -28.84\ {\rm km\ s^{-1}}$, similar to the radial velocity $v_{r,\rm opt} = -28.38\ {\rm km\ s^{-1}}$ measured in 2008 by Tokovinin et al. (2015b).[7]

λ Ara = HD 160032. The inconsistencies with the pressure-dependent Mg Ib triplet lines originally led us to suggest (cf. Fuhrmann et al. 2011b) that this F-type star probably is a binary system. A spectrum that we secured more recently, in 2015 July, shows triangular-shaped absorption line profiles, which is further support for a spectroscopic binary.

This is illustrated in Figure 7 for the Fe I line λ5862.364, where to first approximation we assume a twin binary for λ Ara. In this case, the Balmer line wings lead to $T_{\rm eff,Aa} = T_{\rm eff,Ab} \simeq 6500$ K, and the surface gravities $\log g_{\rm Aa} = \log g_{\rm Ab} \simeq 4.36$ follow from the *Hipparcos* parallax. We further assume microturbulent velocities $\xi_{t,\rm Aa} = \xi_{t,\rm Ab} \simeq 1.60\ {\rm km\ s^{-1}}$, but fix the macroturbulence values, $\zeta_{\rm RT,Aa} = \zeta_{\rm RT,Ab} = 6.4\ {\rm km\ s^{-1}}$, according to the effective temperatures. A single star, as given in the left-hand panel of Figure 7, evidently cannot account for the observed line profile: a projected rotational velocity $v\sin i = 14.3\ {\rm km\ s^{-1}}$ that matches the core fails in the line wings, which in turn require $v\sin i = 17.8\ {\rm km\ s^{-1}}$. A consistent profile fit, however, is achieved in the right-hand panel with a Doppler-shifted binary at $\Delta v_r = 10.0\ {\rm km\ s^{-1}}$ and projected rotational velocities $v\sin i_{\rm Aa} = v\sin i_{\rm Ab} = 13.2\ {\rm km\ s^{-1}}$. For this twin main-sequence star, we find metallicities [Fe/H] $\simeq -0.21$ and [Fe/Mg] $\simeq -0.06$, and stellar masses $M_{\rm Aa} = M_{\rm Ab} \simeq 1.22\,M_\odot$. We note that the twin binary in Figure 7 is not a unique solution for λ Ara from our spectroscopic data. Major photometric differences of the components are unlikely, however, for they should have been visible in the *Hipparcos* astrometry.

At an angular separation of 13″, we briefly mention a faint optical companion 2MASS J17402408-4925088 to λ Ara. A single 1 hr exposure of this source shows that it is likely a distant double-lined giant.

ψ^1 Dra = HD 162003/4. The companion to ψ^1 Dra A that Toyota et al. (2009) first reported to have a 50 $M_{\rm J}$ minimum mass was more recently directly imaged by Endl et al. (2016) as a fairly massive K-type star, only about 3.8 and 4.2 mag fainter at λ8800 and λ6920, respectively. With the radial velocities and orbital elements given in Gullikson et al. (2015) [8], we find that the components of the ψ^1 Dra A subsystem were only $\Delta v_r \simeq 3.9\ {\rm km\ s^{-1}}$ Doppler-displaced when we observed this star in 1998 June (cf. Fuhrmann 2000). With a projected rotational velocity $v\sin i_{\rm Aa} = 11.1\ {\rm km\ s^{-1}}$ for the primary, this explains why ψ^1 Dra A was not immediately visible as a double-lined spectroscopic binary at that epoch. Ignoring the secondary, a reanalysis of ψ^1 Dra Aa provides $T_{\rm eff,Aa} = 6412$ K, $\log g_{\rm Aa} = 4.00$, [Fe/H] $= -0.06$ and [Fe/Mg] $= -0.06$, with the surface gravity fixed from the revised *Hipparcos* parallax. From the photometry in Endl et al. (2016), we assume $\Delta m_V = 4.5$ mag, which, with reference to the VandenBerg et al. (2006) evolutionary tracks, implies a secondary main-sequence position at $T_{\rm eff,Ab} \simeq 4520$ K and a mass $M_{\rm Ab} \simeq 0.72\,M_\odot$. By inclusion of the secondary, the composite model atmosphere analysis shows that its effect on the Balmer line wings amounts to 20 K, meaning that we obtain a

[7] With reference to the very recent *Gaia* DR1 release and the solid $\pi = 44.54 \pm 0.33$ mas parallax for HD 148704, we can now also add the absolute bolometric magnitudes and stellar radii: $M_{\rm bol,Aa} \simeq 5.73$, $M_{\rm bol,Ab} \simeq 6.28$, $R_{\rm Aa} \simeq 0.77\,R_\odot$, $R_{\rm Ab} \simeq 0.68\,R_\odot$, along with two minor adjustments to the surface gravities, $\log g_{\rm Aa} \simeq 4.56$ and $\log g_{\rm Ab} \simeq 4.62$.

[8] The orbital inclination in Table 2 of Gullikson et al. (2015) must be a misprint, however.

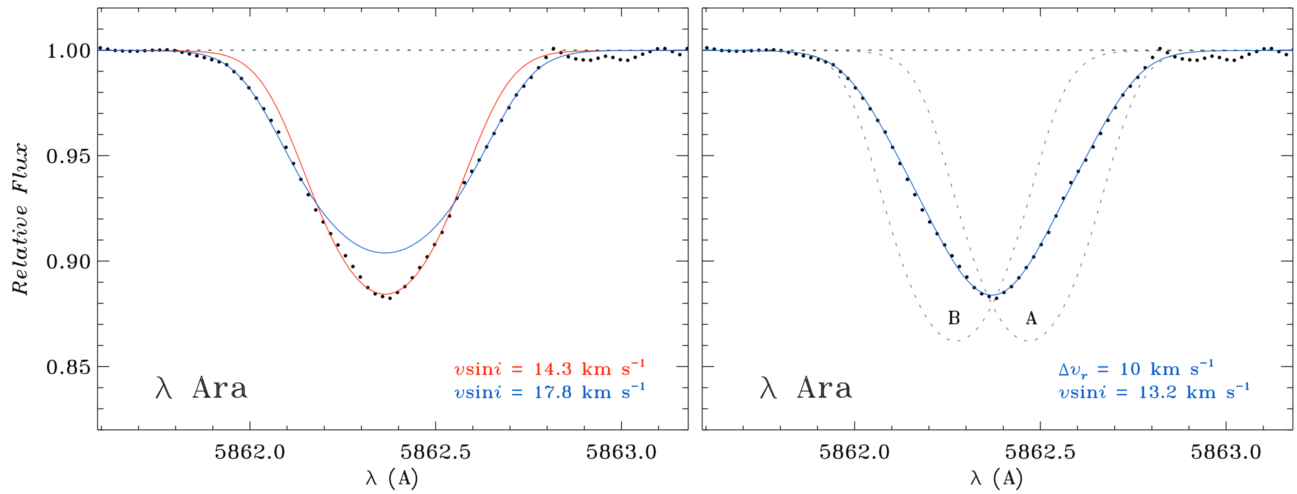

Figure 7. Modeling of the Fe I line λ5862.364 in the high-resolution, high signal-to-noise ratio spectrum (S/N $\simeq$ 500) of the F-type star λ Ara. In the left-hand panel, a single star cannot account for the triangular-shaped line profile. The case of an equal-mass binary, Doppler-displaced at $\Delta v_r = 10.0$ km s^{-1} in the right-hand panel reproduces the observations, however. Gray dotted curves denote the line profiles of the individual components (see text for details).

revised $T_{\mathrm{eff,Aa}} \simeq 6432$ K for the primary. Likewise, the composite analysis results in small abundance corrections to [Fe/H] $\simeq -0.04$ and [Fe/Mg] $\simeq -0.05$, as well as a slightly increased primary mass $M_{\mathrm{Aa}} \simeq 1.46\,M_{\odot}$. The other stellar parameters of interest are as follows: $V_{\mathrm{Aa}} = 4.58$, $M_{V,\mathrm{Aa}} = 2.79$, $M_{\mathrm{bol,Aa}} \simeq 2.72$, $R_{\mathrm{Aa}} \simeq 2.00\ R_{\odot}$, and $V_{\mathrm{Ab}} \simeq 9.08$, $M_{V,\mathrm{Ab}} \simeq 7.29$, $M_{\mathrm{bol,Ab}} \simeq 6.67$, $R_{\mathrm{Ab}} \simeq 0.66\ R_{\odot}$. Because of its importance as the visual companion to ψ^1 Dra A, we also present here a reanalysis of ψ^1 Dra B (cf. Table 1), with essentially consistent iron and magnesium abundances for both stars.

HR 6748 = HD 165185. This is a known member of the young Ursa Major Association. Chini et al. (2014) recently presented the observational evidence for a 12″ distant common-proper-motion red dwarf companion. From FEROS spectra of the primary and secondary we derive consistent radial velocities $v_{r,\mathrm{A}} = +14.96$ km s^{-1} and $v_{r,\mathrm{B}} = +15.03$ km s^{-1} (2015 July 1), and $v_{r,\mathrm{A}} = +15.01$ km s^{-1} (2015 July 3), which confirms their physical association.

HR 6828 = HD 167425. From its kinematics, coronal, and chromospheric activity, this is a rather young visual binary, possibly associated with the Hercules–Lyra Association. For the $\rho = 8''$ distant M-type secondary we measure a radial velocity $v_{r,\mathrm{B}} = +1.11$ km s^{-1}, compared to $v_{r,\mathrm{A}} = +0.47$ km s^{-1} for the primary. A small portion of the spectrum of HR 6828 B is displayed below in Figure 11.

HR 7330 = HD 181321. The primary of this astrometric and spectroscopic binary is a young G-type main-sequence star. The *Hipparcos* parallax, $\pi = 47.95 \pm 1.28$ mas, has been considerably revised to $\pi = 53.10 \pm 1.41$ mas by van Leeuwen (2007). The latter value, however, leads to a slightly subluminous position of HR 7330 Aa in the H-R diagram, and our spectroscopic analysis instead favors a parallax value $\pi = 49.5$ mas. HR 7330 shows kinematics and characteristics very similar to two other southern sources, HR 2882 and 53 Aqr (both discussed in this section). All three stars may be part of a young group that Zuckerman et al. (2013) recently dubbed the "Octans-Near Association." We do not find a trace of the secondary in our spectra, but note that, as a red dwarf, HR 7330 Ab is very likely a pre-main-sequence star.

HR 7674 = HD 190422. Like HR 6748 mentioned above, this is another known member of the young Ursa Major Association (cf. Eggen 1986).

HD 197214. The model atmosphere analysis and the weak coronal (Hünsch et al. 1999) and chromospheric (Ca II H&K) activity imply that HD 197214 is an old Population I star. As such, the Hα line core displays a small but significant 1% filling in, which may be a direct trace of its close Ab component, and if so, HD 197214 Ab would be an ordinary M dwarf.

For the $\rho = 17\farcs6$ distant common-proper-motion red dwarf companion, HD 197214 B, recently discussed in Chini et al. (2014), a 1 hr exposure provides a radial velocity $v_{r,\mathrm{B}} = -18.59$ km s^{-1}, in good agreement with the systemic velocity, $\gamma_{\mathrm{A}} = -19.044 \pm 0.015$ km s^{-1}, of the inner Aa–Ab subsystem that has recently been derived by Willmarth et al. (2016).

HR 8013 = HD 199260. For a star with a nominal age $\tau \sim 3.5$ Gyr, we note a strong X-ray luminosity $L_x = 149.8 \times 10^{27}$ erg s^{-1} (Hünsch et al. 1999), and at the same time a barium overabundance, [Ba/Fe] $= +0.19$, which might both hint at a hidden degenerate companion.

HD 199509. Wittenmyer et al. (2011, 2016) report a long-term linear radial velocity trend from 33 measurements with a time span of more than 15 years from the Anglo-Australian Planet Search. Our FEROS radial velocities, $v_r = -22.20 \pm 0.03$ km s^{-1} (2015 July) and $v_r = -22.00 \pm 0.07$ km s^{-1} (2015 December), deviate by $\Delta v_r = -0.95$ km s^{-1} from the Nordström et al. (2004) radial velocities.[9] For a slowly rotating chromospherically inactive G-type star, this velocity difference is only compatible with stellar, or, for a more eccentric orbit, brown dwarf companion masses.

HR 8061 = HD 200525. This is a known Hyades stream member (Eggen 1960) with a $\rho \simeq 7''$ distant late-type companion, HR 8061 C, in orbit around a close visual binary HR 8061 AB, the latter often considered to consist of near-equal-luminosity subcomponents. However, and as the direct comparison of the neighboring Fe II λ6149.250 and Fe I λ6151.623 lines in Figure 8 show, HR 8061 B is a considerably fainter K-type companion, on account of its strong contribution in the blue wing of the Fe I absorption line, and the lack thereof with the Fe II line, which is dominated by HR 8061 A. Recent speckle

[9] This includes a $\Delta v_r = +0.38$ km s^{-1} zero-point offset for common slowly rotating and presumably single stars.

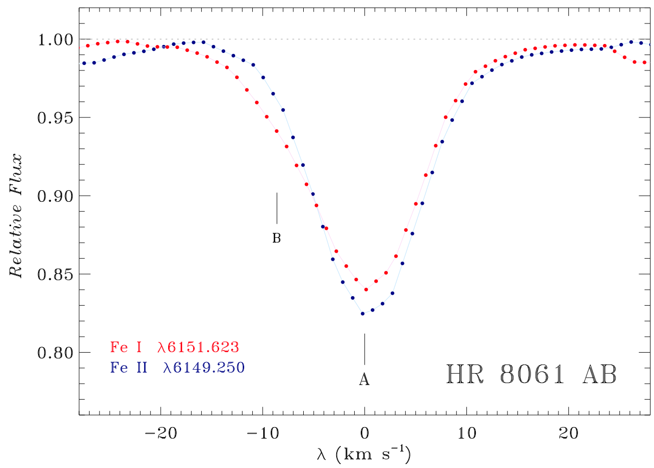

Figure 8. Line profiles of Fe II $\lambda6149.250$ (blue) and Fe I $\lambda6151.623$ (red) for the late-F visual binary HR 8061 AB, a young Hyades stream member and often purported near-equal-luminosity object. At this 2015 July 2 observation, the components were Doppler-shifted at Δv_r(A–B) = +8.6 km s^{-1}, and the mostly symmetric Fe II line, as opposed to the skewed Fe I line, is direct evidence for a much fainter K-type secondary.

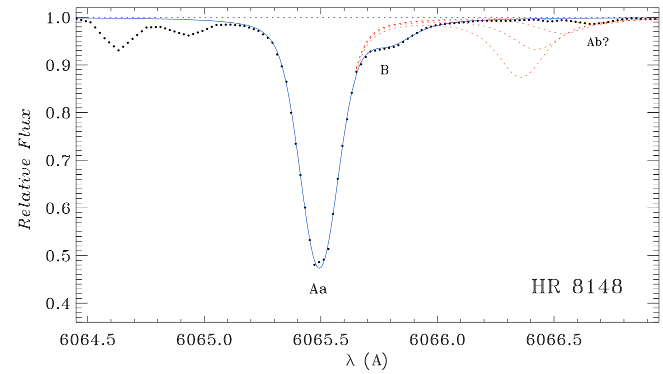

Figure 9. Modeling of the strong Fe I line $\lambda6065.493$ for the triple star HR 8148. The high-resolution spectrum was exposed on 2015 June 29 at phase $\Phi \simeq 0.26$ of the inner $P = 21.3$ days Aa–Ab spectroscopic orbit. The contribution of the three magnitudes fainter visual B component, separated at that epoch at $\rho \simeq 0\farcs6$ and redshifted at $\Delta v_{r,\rm B} = +14$ km s^{-1}, is shown with the composite spectrum synthesis (dark blue). The red dotted curves illustrate four cases of a $\Delta m_V = 2.0$, 3.0, 4.0, and 5.0 mag fainter Ab red dwarf companion. There is weak evidence that the faintest of these cases with $M_{\rm Ab} \simeq 0.40\,M_\odot$ might apply.

interferometry by Tokovinin et al. (2010) at epoch 2008.7696 provides $\Delta m_y = 3.17$ mag and $\rho = 0\farcs29$ for HR 8061 AB. In view of the Hyades stream membership described above with a likely super-solar metallicity, the differential photometry applied to evolutionary tracks then implies a $T_{\rm eff,B} \simeq 4450$ K main-sequence position for HR 8061 B, and from the composite Balmer line wings a $T_{\rm eff,A} \simeq 6050$ K main-sequence position follows for HR 8061 A.

As Figure 8 also shows, our 2015 July 2 single-epoch spectroscopic observation of HR 8061 AB is not resolved, and the preliminary orbital solution by Goldin & Makarov (2006) with $P \simeq 6$ years suggests that resolved spectra may only be possible near periastron passage. Nevertheless, the above effective temperatures, along with the surface gravities $\log g_{\rm A} \simeq 4.36$ and $\log g_{\rm B} \simeq 4.66$ from the *Hipparcos* astrometry, allow for a fairly robust composite model atmosphere analysis with abundances [Fe/H] $\simeq +0.13$ and [Fe/Mg] $\simeq +0.04$, and with only some uncertainty on the projected rotational velocities that we provisionally estimate to $v \sin i_{\rm A} \sim 6.3$ km s^{-1} and $v \sin i_{\rm B} \sim 4.3$ km s^{-1}. For the stellar masses, the VandenBerg et al. (2006) evolutionary tracks then provide $M_{\rm A} \simeq 1.15\,M_\odot$ and $M_{\rm B} \simeq 0.73\,M_\odot$. With the radial velocities, $v_{r,\rm A} = -7.25$ km s^{-1} and $v_{r,\rm B} = -15.85$ km s^{-1}, the systemic velocity for the HR 8061 AB subsystem follows to be $\gamma_{\rm AB} = -10.58$ km s^{-1}, with an uncertainty of about 0.5 km s^{-1}. The other stellar parameters of relevance are $V_{\rm A} \simeq 5.72$, $M_{V,\rm A} \simeq 4.24$, $M_{\rm bol,A} \simeq 4.15$, $R_{\rm A} \simeq 1.17\,R_\odot$, and $V_{\rm B} \simeq 8.89$, $M_{V,\rm B} \simeq 7.40$, $M_{\rm bol,B} \simeq 6.72$, $R_{\rm B} \simeq 0.66\,R_\odot$.

For the faint and distant red dwarf HR 8061 C, a single 1 hr exposure results in a radial velocity $v_{r,\rm C} = -8.64$ km s^{-1}. Provided there is no other hidden companion, and assuming a stellar mass $M_{\rm C} \sim 0.50\,M_\odot$, the systemic velocity of the HR 8061 system should be close to $\gamma \simeq -10.2$ km s^{-1}.

HD 202628. The basic characteristics of this star are very close to that of the Sun, the only exception being a weak chromospheric activity. The modest $\lambda6707$ lithium absorption in the spectrum then implies that HD 202628 is likely not as old as our parent star.

HR 8148 = HD 202940. As with HD 148704 above, the space velocity, $U/V/W = +41/-27/+47$ km s^{-1}, and a low level of chromospheric and coronal activity (Hünsch et al. 1999) are both suggestive of an old Population I member. However, and unlike the $P = 31.8$ day spectroscopic binary HD 148704, the $P = 21.3$ day spectroscopic binary HR 8148 (Bopp et al. 1970; Abt & Willmarth 2006) has a known visual B component with a semimajor axis of about $2\farcs5$. This outer orbit of HR 8148 was first assessed as fairly circular ($e = 0.06$) with a period $P = 349.2$ years (Hale 1994), but soon hereafter revised to $P = 261.6$ years and $e = 0.424$ in Jasinta (1997). Recently, it was found that the visual orbit is highly eccentric at $e = 0.898$, and the period has been further reduced to $P = 157.5$ years (Tokovinin et al. 2014). A surprisingly large change in the systemic velocity of 1.5 ± 0.3 km s^{-1} in 2001–2003 was found by Abt & Willmarth (2006) for the inner $P = 21.3$ day subsystem. This could mean that there is another, fourth component for HR 8148, but it appears difficult to reconcile this with the revised extreme eccentricity of the outer orbit.

At the 2015 June 29 epoch of our observations, the three magnitude fainter HR 8148 B had closed in to $\rho \simeq 0\farcs6$ (Tokovinin et al. 2014), such that most but not all of its light also passed the fiber entrance aperture of the spectrograph. From the *Hipparcos* photometry and given that HR 8148 is slightly metal-poor (see below), we can estimate that this visual component—if single—should have an approximate effective temperature $T_{\rm eff,B} \simeq 4070$ K and mass $M_{\rm B} \simeq 0.58\,M_\odot$. The composite spectrum synthesis for the strong Fe I line $\lambda6065.493$ in Figure 9 shows that HR 8148 B is redshifted at $\Delta v_{r,\rm B} = +14$ km s^{-1} and causes a weak but significant contribution. On the other hand, and with our observations of the inner orbit at phase $\Phi \simeq 0.26$ with $v_{r,\rm Aa} = -31.86$ km s^{-1}, we also searched for a trace of the tertiary Ab component of HR 8148, but with likely only limited success. This is demonstrated in Figure 9, with the red curves that delineate four cases of a 2.0–5.0 mag fainter main-sequence companion. The faintest of these cases may apply here, i.e., with a very weak absorption of an $M_{\rm Ab} \simeq 0.40\,M_\odot$ M dwarf, redshifted at $\Delta v_{r,\rm Ab} = +59\ \rm km\ s^{-1}$.

Ignoring this uncertain tertiary contribution, the composite modeling of HR 8148 Aa and B proceeds in a similar manner as with HD 148704 above. It is found that HR 8148 possesses a fairly similar chemistry at [Fe/H] $\simeq -0.26$ and [Fe/Mg] $\simeq -0.08$, albeit with a somewhat hotter and more massive primary at $T_{\rm eff,Aa} = 5470$ K, $\log g_{\rm Aa} = 4.46$, and $M_{\rm Aa} = 0.85\,M_\odot$. The mass of the Ab component is then constrained to $0.31 \leqslant M_{\rm Ab} \leqslant 0.40\,M_\odot$ from the Abt & Willmarth (2006) mass function and with reference to Figure 9. In view of the considerable $e = 0.362$ eccentricity of the inner orbit (Abt & Willmarth 2006) and since the mass of HR 8148 Ab does not follow the Rappaport et al. (1995) period—white dwarf mass relation, it is in all likelihood an M-type red dwarf.

HD 203244. The chromospheric activity and kinematics together with the iron and barium abundances let us conclude that this astrometric ($P = 1060$ day) and spectroscopic binary[10] belongs to the young stars of the Ursa Major Association. There are no traces of blueshifted secondary absorption lines on our single 2015 December 21 spectrum, which means that it cannot affect the derived abundances. The effective temperature from the Balmer line wings and the surface gravity that follows from the iron ionization equilibrium, however, lead to a slight inconsistency with the astrometric parallax. The effect amounts to 30 K, which suggests the presence of a five or six magnitudes fainter M-type secondary on the Balmer line wings. This assessment also agrees with the *Hipparcos* astrometric orbit that provides a $M_{\rm Ab} \simeq 0.40\,M_\odot$ secondary mass, although some uncertainty remains here with the luminosity of the Ab component, since it may still be on its pre-main-sequence track. In Table 1 we account for the consistent $T_{\rm eff}/\log g$ pair for HD 203244 Aa, such that the effect of the secondary becomes negligible for the given stellar parameters.

HR 8526 = HD 212168. Until recently only known as a visual binary (cf. Raghavan et al. 2010), HR 8526 consists of at least four to six components. In the first place, we mention a $\rho = 4.4'$ distant M-dwarf companion that was found by Caballero & Montes (2012), which they consider to be itself an unresolved binary candidate. Next, the G-type primary, HR 8526 A, is a spectroscopic binary in Nordström et al. (2004), although subsequent regular monitoring by Wittenmyer et al. (2011, 2016) shows constant radial velocities. This controversial result might be explained with a long-period low-mass or brown dwarf companion in an eccentric orbit. A very memorable example of this type was most recently presented for the nearby Population II star HD 18757 by Bouchy et al. (2016, their Figure 5). Last, the 21″ distant B component is a visual (Tokovinin et al. 2015a) and double-lined spectroscopic subsystem. For our single 2015 June 29 epoch spectrum we derive $v_{r,\rm Ba} = +19.4\ \rm km\ s^{-1}$, whereas the fainter and only partly resolved Bb companion is blueshifted at $v_{r,\rm Bb} \simeq +10.2\ \rm km\ s^{-1}$. With preliminary mass estimates $M_{\rm Ba} \sim 0.67\,M_\odot$ and $M_{\rm Bb} \sim 0.54\,M_\odot$, an approximate systemic velocity $\gamma_{\rm B} \simeq +15.3\ \rm km\ s^{-1}$ follows for this subsystem.

53 Aqr = HD 212697/8. As has been noted by Alden (1936), the visual binary has a highly eccentric orbit whose

[10] The "constant radial velocities" stated in Raghavan et al. (2010) are in direct contradiction to the Nordström et al. (2004) radial velocities of HD 203244. In line with the latter work, our single-epoch measurement, $v_{r,\rm Aa} = +22.50\ \rm km\ s^{-1}$, suggests a primary semi-amplitude of 5–10 km s^{-1}.

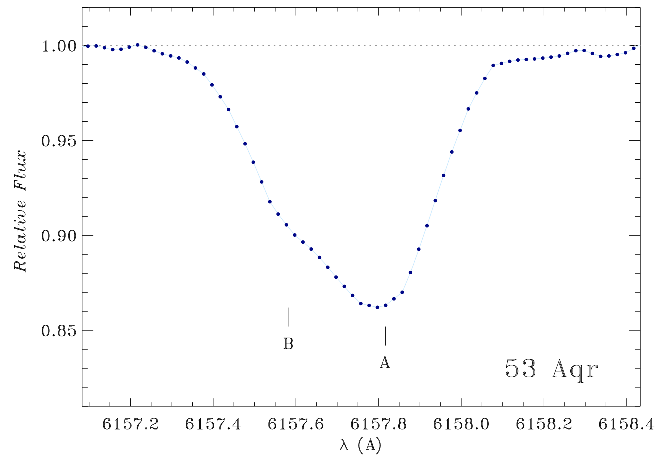

Figure 10. Spectral line profile of Fe I λ6157.733 for the young and near-equal-mass G-type visual binary 53 Aqr, taken on 2015 July 1. This near periastron epoch spectrum shows the visual components Doppler-shifted at Δv_r(A–B) = +11.6 km s^{-1}. Both 53 Aqr A and B possess enhanced projected rotational velocities $v \sin i_{\rm A} \simeq 8.0\ \rm km\ s^{-1}$ and $v \sin i_{\rm B} \simeq 6.8\ \rm km\ s^{-1}$. The strong asymmetry of the composite line profile mostly reflects the loss of light for the 1.″3 displaced 53 Aqr B at the fiber entrance of the spectrograph.

angular separation steadily decreased since it was first observed in the early nineteenth century with more than 12″ at that time, down to 1.″3 at present, close to periastron epoch. As a result, our spectroscopic observations with a 2″ fiber diameter include both components with a major loss of light for the secondary, however, as displayed in Figure 10.

In spite of this disadvantage for a quantitative composite model atmosphere analysis, other solid constraints still allow for a fairly precise determination of the stellar parameters of 53 Aqr A and B. The most basic observation refers to Pasquini et al. (1994, their Figure 2) and shows the A and B components both with a strong λ6707 lithium absorption and enhanced rotational velocities (with $v \sin i_{\rm B} < v \sin i_{\rm A}$). Given that both 53 Aqr A and B are early G-type stars, this immediately implies that they must be young objects, very likely comparable to those of the local Ursa Major and Hercules–Lyra Associations (cf. Fuhrmann 2004, Figures 17 and 30) with ages of only a few 100 Myr.

A second important constraint for 53 Aqr A and B arises from the *Hipparcos* photometry with $\Delta H_p = 0.15$ mag. In terms of effective temperatures this translates into $\Delta T_{\rm eff} \simeq 70$ K for bona fide coeval components and results in $T_{\rm eff,A} \simeq 5875$ K and $T_{\rm eff,B} \simeq 5805$ K from the composite Balmer line wings. At this point, the *Hipparcos* parallax provides surface gravities $\log g_{\rm A} \simeq 4.45$ and $\log g_{\rm B} \simeq 4.48$, as expected for young main-sequence stars. For the composite abundance analysis, we assume microturbulent velocities $\xi_{t,\rm A} \simeq 1.00\ \rm km\ s^{-1}$ and $\xi_{t,\rm B} \simeq 0.95\ \rm km\ s^{-1}$, with reference to similar stars of the Ursa Major and Hercules–Lyra Associations. For the macroturbulent velocities, in turn, we adopt $\zeta_{{\rm RT},A} = 4.0\ \rm km\ s^{-1}$ and $\zeta_{{\rm RT},B} = 3.7\ \rm km\ s^{-1}$, according to the derived effective temperatures. In the next step, the modeling of the iron lines shows that about 40% of the light of 53 Aqr B was lost at the fiber entrance (with the implicit assumption, however, that the primary and secondary have the same iron abundance). For the iron and magnesium lines we then derive [Fe/H] $\simeq -0.10$ and [Fe/Mg] $\simeq +0.02$, and the projected rotational velocities follow to $v \sin i_{\rm A} \simeq 8.0\ \rm km\ s^{-1}$ and $v \sin i_{\rm B} \simeq 6.8\ \rm km\ s^{-1}$, both velocities with uncertainties of at least 1.0 km s^{-1}. At the given metallicities, evolutionary tracks lead to stellar masses

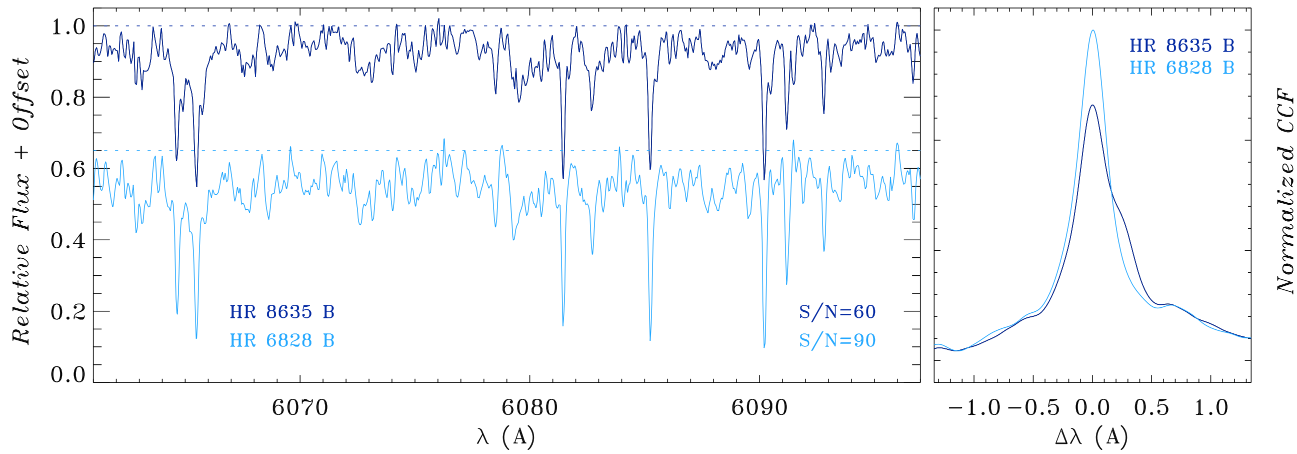

Figure 11. Left: portion of the optical spectra of the M dwarfs HR 6828 B and HR 8635 B that discloses the latter as a double-lined spectroscopic binary with a $\Delta v_r = +14.0$ km s^{-1} redshifted Bb component; note also the correspondingly less deep absorption lines for HR 8635 B. Right: the cross-correlation function of HR 6828 B is symmetric, that of HR 8635 B displays a composite profile.

$M_{\rm A} \simeq 1.06\,M_\odot$ and $M_{\rm B} \simeq 1.03\,M_\odot$, and the set of basic stellar parameters for 53 Aqr A and B complements as follows: $V_{\rm A} = 6.24$, $M_{V,{\rm A}} = 4.71$, $M_{\rm bol,A} \simeq 4.58$, $R_{\rm A} \simeq 1.02\ R_\odot$, and $V_{\rm B} = 6.39$, $M_{V,{\rm B}} = 4.86$, $M_{\rm bol,B} \simeq 4.73$, $R_{\rm B} \simeq 0.98\ R_\odot$.

We note that Willmarth et al. (2016) find an additional short-term $P = 257$ day spectroscopic orbit for the 53 Aqr B secondary. The census for 53 Aqr therefore amounts to at least three components.

Recently, Zuckerman et al. (2013) suggested that 53 Aqr is a possible member of a group of young stars, which they call the "Octans-Near Association" (cf. also Figure 10 in P3). While there is indeed some uncertainty on the kinematics of 53 Aqr from both its proper motion (on account of the highly eccentric visual orbit) and the uncertain systemic velocity, we note that 53 Aqr shares many characteristics with the nearby young G-type stars HR 2882 and HR 7330 discussed above.

υ Aqr = HD 213845. With a projected rotational velocity that we measure as $v \sin i_{\rm A} = 36 \pm 1$ km s^{-1}, there remain only a few suitable iron lines for a model atmosphere analysis of the F-type primary. From the Balmer line wings we derive an effective temperature $T_{\rm eff,A} = 6513$ K, and from the *Hipparcos* parallax a surface gravity $\log g_{\rm A} = 4.25$. For the iron abundance we get [Fe/H] $\simeq +0.11$, which leads to a mass $M_{\rm A} \simeq 1.35\,M_\odot$ and an age of about 1 Gyr. The latter is somewhat at odds with the kinematics that promotes a Hercules–Lyra Association membership. However, it seems we may not exclude that the primary is itself an Aa–Ab binary on account of some variabilities with the radial velocity and the width of the cross-correlation function that both require further attention.

HR 8635 = HD 214953. A high-resolution spectrum of the 8″ distant M-dwarf secondary HR 8635 B secured on 2015 December 27 displays two M dwarfs, Doppler-shifted at $\Delta v_r = +14.0$ km s^{-1}, with $v_{r,{\rm Ba}} = +12.1$ km s^{-1} and $v_{r,{\rm Bb}} = +26.1$ km s^{-1}. Figure 11 shows a portion of the spectrum of HR 8635 Ba and Bb in comparison to the M dwarf HR 6828 B.

HD 218687. In view of its kinematics and chromospheric activity, the star might be mistaken as a young Ursa Major Association member. The chromospheric activity, however, is solely caused by the short $P = 3.63$ day circularized orbit (Griffin 2001), and the lack of the Li I λ6707 resonance line as well as the *Hipparcos*-based surface gravity $\log g_{\rm Aa} = 4.37$ both demonstrate that the star cannot be young. The lack of a barium overabundance particularly demonstrates that neither can it be part of the Ursa Major Association. At $T_{\rm eff,Aa} = 5887$ K and [Fe/H]$= -0.14$, the VandenBerg et al. (2006) tracks in fact provide a turnoff stage of evolution for the primary, a mass $M_{\rm Aa} = 1.00\,M_\odot$, and an age of about 6 Gyr.

For one of our HD 218687 A spectra, taken at orbital phase $\Phi = 0.06$, we obtain Doppler offsets of Δv_r(Ab–Aa) $= -49$ to -63 km s^{-1} for a 3–5 mag fainter main-sequence secondary. A similar comparison as in Figure 9 shows, however, that we can exclude any such companion in the spectrum. Upon the reasonable assumption of bound rotation as well as rotational and orbital coplanarity for the close pair, the orbital inclination likely amounts to $i = 42°$. The Griffin (2001) mass function then implies a $M_{\rm Ab} = 0.28\,M_\odot$ secondary, too faint to be visible in the optical spectra.

Because of the short Aa–Ab orbital period, it is no surprise that HD 218687 A also possesses a distant common-proper-motion companion. For this 31″ separated tertiary component, HD 218687 B, Griffin (2001) already demonstrated that it shares the radial velocity with the systemic velocity of the inner Aa–Ab subsystem.

γ Tuc = HD 219571. The F-type primary of this astrometric binary is a slightly more massive version of the bright star Procyon, with a projected rotational velocity $v \sin i_{\rm A} = 80$ km s^{-1} as the major obstacle for an accurate model atmosphere analysis, however. While the effective temperature, $T_{\rm eff,A} = 6504$ K, and surface gravity, $\log g_{\rm A} = 3.81$, can therefore be derived in the usual manner from the Balmer line wings and the *Hipparcos* parallax, there are no suitable Fe II lines in our spectra. Hence, and similar to the fast-rotating κ Tuc above, we have to work with Fe I lines and apply an approximate abundance correction Δ[Fe/H] $\simeq +0.20$ dex (cf. Steffen 1985; Fuhrmann et al. 1997) that leads to [Fe/H] $\simeq -0.15$. With these parameters, we obtain a primary mass $M_{\rm A} \simeq 1.59\,M_\odot$, a stellar radius $R_{\rm A} = 2.60\ R_\odot$, and a bolometric magnitude $M_{\rm bol,A} = 2.10$.

The observations of γ Tuc A reveal line profile variabilities very similar to those we have discussed for other F-type stars in P1. It will be of interest to see if these are non-radial γ Dor-type pulsations, and if so, whether they are driven by the hidden companion. The radial velocities that we measure from 11 observations of γ Tuc A are in the range from +1.8 to +7.2 km s^{-1} with an average $\langle v_{r,\mathrm{A}}\rangle = +5.3$ km s^{-1}.

HD 222335. The star is not mentioned in the *ROSAT* all-sky catalog (Hünsch et al. 1999) of nearby stars, but it shows a weak chromospheric signature from Ca II H&K and Hα. Its position in the H-R diagram appears slightly above the main sequence, which might be suggestive of a faint companion.

4. Stellar Multiplicities

A quantitative understanding of star formation as a function of mass, metal enrichment, or environment, as well as the involved stellar multiplicities, is of fundamental importance in astrophysics. The field stars we observe in the solar neighborhood at highest resolution are mostly dissolved objects of former star clusters or associations, and in this process are also subject to dynamical interaction that can lead to ascending or descending stellar multiplicities. Field stars still retain important information in terms of their chemistry, kinematics, rotation, ages, and the stellar populations they belong to. The individual identification of Population II stars, for instance, has been a central issue from the outset of our survey. The investigation of these ancient long-lived stars leads to important insights on the dynamics, the star formation rate, and chemical enrichment of the early Milky Way, aspects that have all been addressed in the accompanying work on the stellar populations (P3). The study of their multiplicities may lead to further insight into the star formation process, which could have been qualitatively very different compared to the much younger Population I stars (e.g., Kroupa 2002).

For the rather short-lived F-type stars, which are essentially all Population I members, the stellar multiplicities have been discussed in P1 and P2, with a 25% inventory of triple or higher level systems, and 67% of the F-type stars being non-single. By inclusion of the less massive G-type stars with this work, a significant fraction of long-lived sources now becomes part of the census, and we have to carefully distinguish between Population I and II stars, some stars being even intermediate to both populations, and we discuss their multiplicities separately.

As we have shown in P3, there are 22 Population II stars in the survey and another 9 intermediate-disk stars with ages of about 10 Gyr, intermediate to that of Population I and Population II. In continuation of P1 and P2, we first discuss the stellar multiplicities of the survey Population I stars, and then compare the relevant findings with the old Population II and intermediate-disk stars.

4.1. Population I Stars

The multiplicities and masses of the 391 Population I stars that we count with this survey are set out in Table 5. Note that we refer to primary masses in case of binaries or higher level systems and that the masses are mostly based on model atmosphere analyses and stellar evolutionary tracks, as with the stars discussed in Section 3 of this work. For the many relevant details on individual stars we refer here to our previous contributions to this survey in the literature. Early-type stars with $T_{\mathrm{eff}} \geqslant 7000$ K, but also a few fast rotators below this effective temperature, were generally not part of our analyses. Some of them have accurate masses from orbital elements, but for others the lack of model atmosphere analyses and the impact of stellar rotation are both sources of uncertainty for their stellar masses. Likewise, the more evolved giant stars (except for the Population II giant Arcturus) were not part of our analyses and some of the given masses are therefore only rough estimates. More importantly, however, these giant stars have in all likelihood been subject to substantial mass loss, and, as a result, there is no reliable information on their birth mass. However, and as has been argued in P2, most of the giants still carry the multiplicity information, and we therefore prefer to include them for the census.

While the giant star masses are then likely shifted toward lower mass bins, mass transfer from nuclear or orbital evolution, in turn, can lead to stars with higher masses. This may, for instance, be the case with Regulus, the only B-type star of the survey, but likely an A-type star at birth. Similarly, today we observe α Tri as a $P = 1.73$ day short-period F-type star, but upon further evolution it may soon become an A-type star. The well-known X-ray source YY Gem currently is a 0.6 $M_{\odot}$ M-type twin binary with a $P = 0.81$ day orbital period, but a future merger may lead to a single bright F-type star. If, on the other hand, we consider the comparatively wide Sirius system ($P = 50.1$ years) with its 2.0 $M_{\odot}$ A-type primary and the 1.0 $M_{\odot}$ white dwarf secondary, we must expect that this massive remnant was a B-type star at birth. Hence, Sirius A is not the very relevant component for our census, and given that Sirius A is itself a likely case for wind accretion, we may not even know its birth mass either (cf. Fuhrmann et al. 2014).

Along with other examples of this kind, we can ask how many of the survey A-type stars might have been F- or G-type stars at birth, or how many of the F- and G-type stars were former K- or M-type dwarfs. Since our census will mostly be concerned with solar-type stars, the two dozen A-type stars are not very relevant for the present work. Moreover, the few giant stars are of no real concern in this context. However, and as we have pointed out in P3, the hope that mass-transfer systems and blue straggler stars may not be important for the less massive solar-type stars of the survey is not fulfilled, the case of the Population I star Gl 504 (59 Vir) being a recent constructive example (Fuhrmann & Chini 2015a). For the Population II stars, whose evolution took place on a much longer timescale, this indeed affects a significant fraction of the whole population.

We note at this point that a systematic discussion of orbital elements or companion masses is beyond the scope of the present work. For many systems there are large uncertainties on these parameters, the orbital "evolution" of HR 8148 being a good example, or the case of HR 8526, both systems discussed in Section 3 above. Likewise, companion masses are often only lower limits (cf. the case of ψ^1 Dra Ab above), and it appears that we have just started to appreciate that many companions are themselves part of close subsystems (e.g., Tokovinin 2014b; Riddle et al. 2015). Most importantly, the contribution of degenerate companions continues to be a major source of uncertainty (e.g., Ferrario 2012; Holberg et al. 2013; Katz et al. 2014; Fuhrmann et al. 2016) that remains literally in the dark.

The stellar multiplicities that we can present in Figure 12 and Table 6 are in this sense only a momentary account that will certainly receive many revisions in the years to come. However, and except for a few controversial systems, these revisions can only proceed in one direction: the fraction of single stars can only decrease, while triple and higher level systems will very likely receive more weight. Even with the

Table 5
Multiplicity Census of the Survey Population I Stars

Object	HR	HD	Mass ($M_\odot$)	N	Object	HR	HD	Mass ($M_\odot$)	N	Object	HR	HD	Mass ($M_\odot$)	N
Sun			1.00	1		5	123	1.04	3		8	166	0.99	1
Caph	21	432	1.91	1	6 Cet	33	693	1.07	1	θ Scl	35	739	1.25	2
		870	0.89	1			1237	0.98	2			1273	0.86	2
	72	1461	1.09	1			1562	0.95	2	ζ Tuc	77	1581	0.98	1
9 Cet	88	1835	1.10	1	β Hyi	98	2151	1.11	1	κ Phe	100	2262	1.77	1
13 Cet	142	3196	1.19	3		159	3443	0.89	2		176	3823	1.05	2
	209	4391	1.00	3	η Cas	219	4614	0.96	2	64 Psc	225	4676	1.21	2
		4747	0.85	2	ϕ^2 Cet	235	4813	1.10	1			4915	0.91	1
	244	5015	1.17	1	37 Cet	366	7439	1.21	3	ν Phe	370	7570	1.17	1
		7590	1.03	1	κ Tuc	377	7788	1.36	4			9407	0.97	1
		9540	0.93	1	υ And	458	9826	1.27	2			10086	1.03	1
	483	10307	1.02	2		506	10647	1.09	1		511	10780	0.88	1
χ Cet	531	11171	1.47	3	α Tri	544	11443	1.70	2	β Ari	553	11636	2.00	2
χ Eri	566	11937	1.58	2			12051	1.05	2	α Hyi	591	12311	2.05	2
		12846	0.86	1	α Ari	617	12929	1.00	1	δ Tri	660	13974	0.99	2
	672	14214	1.21	2		683	14412	0.82	1	κ For	695	14802	1.13	3
ϵ Cet	781	16620	1.30	2		784	16673	1.16	2	12 Per	788	16739	1.38	2
84 Cet	790	16765	1.15	2	θ Per	799	16895	1.18	2	γ Cet	804	16970	2.00	3
ι Hor	810	17051	1.16	1	τ^1 Eri	818	17206	1.27	2	51 Ari		18803	1.04	1
ι Per	937	19373	1.11	1	94 Cet	962	19994	1.30	3	α For	963	20010	1.21	3
		20407	0.92	1	κ^1 Cet	996	20630	1.01	1	ζ^2 Ret	1010	20807	0.96	2
κ Ret	1083	22001	1.37	2	10 Tau	1101	22484	1.08	1	δ Eri	1136	23249	1.27	1
τ^6 Eri	1173	23754	1.43	1			24409	1.00	3			24496	0.92	2
	1249	25457	1.23	1	39 Tau	1262	25680	1.05	2	50 Per	1278	25998	1.28	3
	1294	26491	0.97	2		1322	26923	1.10	2	γ Dor	1338	27290	1.52	1
ϵ Ret	1355	27442	1.09	2	Aldebaran	1457	29139	1.40	2	α Cae	1502	29875	1.46	3
58 Eri	1532	30495	1.05	1	π^3 Ori	1543	30652	1.30	1			32778	0.85	3
ζ Dor	1674	33262	1.09	2		1686	33564	1.32	1	Capella	1708	34029	2.57	4
λ Aur	1729	34411	1.05	1	111 Tau	1780	35296	1.16	3			36435	0.91	1
γ Lep	1983	38393	1.18	2	ζ Lep	1998	38678	1.87	1		2007	38858	0.91	1
β Pic	2020	39060	1.75	1	π Men	2022	39091	1.07	1	χ^1 Ori	2047	39587	1.07	2
		39855	0.82	2	η Lep	2085	40136	1.47	1	β Aur	2088	40183	2.36	3
		42618	0.94	1		2208	42807	0.97	1	71 Ori	2220	43042	1.29	1
	2225	43162	0.98	4	74 Ori	2241	43386	1.27	1		2251	43587	1.03	4
α Men	2261	43834	0.95	2		2318	45184	1.04	1			45270	1.09	1
		45391	0.87	1		2401	46588	1.08	2	ν^2 CMa	2429	47205	1.19	1
	2468	48189	1.09	3	ψ^5 Aur	2483	48682	1.12	1	ξ Gem	2484	48737	1.70	1
Sirius	2491	48915	2.02	2		2500	49095	1.09	3	37 Gem	2569	50692	1.00	1
		51419	0.89	1		2643	52711	0.99	1			53143	0.96	1
	2721	55575	0.95	1		2740	55892	1.38	1	δ Gem	2777	56986	1.60	3
22 Lyn	2849	58855	1.09	1	ρ Gem	2852	58946	1.41	3			59468	0.96	1
	2882	59967	1.02	1	Castor	2891	60179	2.27	6	Procyon	2943	61421	1.48	2
Pollux	2990	62509	2.02	1		2997	62613	0.87	1		2998	62644	1.38	2
		63433	0.99	1	9 Pup	3064	64096	0.96	2		3079	64379	1.23	2
μ^2 Cnc	3176	67228	1.21	1	ρ Pup	3185	67523	1.90	1	18 Pup	3202	68146	1.18	3
ζ^1 Cnc	3208	68257	1.28	5		3259	69830	0.87	1	χ Cnc	3262	69897	1.10	1
	3309	71148	1.00	1	α Cha	3318	71243	1.49	1	π^1 UMa	3391	72905	1.04	1
		73350	1.05	1		3430	73752	1.21	3	δ Vel	3485	74956	2.43	3
ρ^1 Cnc	3522	75732	1.08	2			75767	0.96	4		3538	76151	1.05	1
ι UMa	3569	76644	1.68	4		3570	76653	1.23	1	10 UMa	3579	76943	1.46	2
σ^2 UMa	3616	78154	1.31	2		3625	78366	1.08	1	16 UMa	3648	79028	1.11	2
π^1 Cnc	3650	79096	0.88	4	23 UMa	3757	81937	1.78	2	τ^1 Hya	3759	81997	1.38	3
θ UMa	3775	82328	1.41	2	ψ Vel	3786	82434	1.56	2	11 LMi	3815	82885	1.13	2
	3862	84117	1.12	1	15 LMi	3881	84737	1.14	1	20 LMi	3951	86728	1.08	2
Regulus	3982	87901	4.15	4		4013	88742	1.03	1	39 Leo	4039	89125	1.04	2
		89269	0.88	1	40 Leo	4054	89449	1.40	3		4084	90089	1.27	2
		90156	0.88	1			90343	0.97	1		4102	90589	1.45	1
36 UMa	4112	90839	1.08	2		4134	91324	1.18	2			92719	0.94	1
47 UMa	4277	95128	1.03	1	Merak	4295	95418	2.51	1			96064	0.92	3
	4345	97334	1.08	3	δ Leo	4357	97603	2.05	1	ξ UMa	4375	98231	0.98	5
		98281	0.80	1	ι Leo	4399	99028	1.70	3	83 Leo	4414	99491	1.12	2
88 Leo	4437	100180	1.06	2		4486	101177	0.97	3	61 UMa	4496	101501	0.94	1
	4525	102438	0.85	1	Denebola	4534	102647	1.88	2	β Vir	4540	102870	1.27	1
	4587	104304	1.10	2	η Cru	4616	105211	1.52	2	α Crv	4623	105452	1.39	1
		105590	0.97	2			105631	1.00	1	Megrez	4660	106591	2.06	1
	4767	108954	1.03	1	η Crv	4775	109085	1.47	1	β CVn	4785	109358	0.93	1
γ Vir	4825	110379	1.40	2	10 CVn	4845	110897	0.89	1		4864	111395	1.01	1
	4867	111456	1.22	2			113283	0.98	1	α Com	4968	114378	1.19	2
	4979	114613	1.27	1	β Com	4983	114710	1.06	1		4989	114837	1.14	2
		114853	0.90	2	59 Vir	5011	115383	1.16	2	61 Vir	5019	115617	0.92	1
ι Cen	5028	115892	2.10	1			116956	0.94	1		5070	117043	1.02	1

Table 5
(Continued)

Object	HR	HD	Mass ($M_\odot$)	N	Object	HR	HD	Mass ($M_\odot$)	N	Object	HR	HD	Mass ($M_\odot$)	N
70 Vir	5072	117176	1.06	1	ζ Vir	5107	118098	1.98	2	1 Cen	5168	119756	1.52	1
τ Boo	5185	120136	1.42	2		5209	120690	1.01	2	η Boo	5235	121370	1.67	2
	5243	121560	1.02	1		5273	122742	0.92	2	θ Cen	5288	123139	1.27	1
		124292	0.85	1		5325	124580	1.06	1	ι Vir	5338	124850	1.54	4
	5356	125276	0.93	2		5384	126053	0.91	2	θ Boo	5404	126660	1.26	2
	5423	127334	1.07	1	σ Boo	5447	128167	1.27	1			128400	0.98	1
α^1 Cen	5459	128620	1.13	3			128642	0.87	2	α Cir	5463	128898	1.71	2
		128987	0.97	1	μ Vir	5487	129502	1.48	2			130042	0.89	2
α^2 Lib	5531	130841	1.92	4		5534	130948	1.05	3	ξ Boo	5544	131156	0.91	2
44 Boo	5618	133640	0.98	3		5632	134060	1.05	1	45 Boo	5634	134083	1.32	1
		136923	0.83	1	η CrB	5727	137107	1.24	3			137763	0.92	3
Alphecca	5793	139006	2.58	2		5825	139664	1.33	1		5829	139777	1.03	2
ψ Ser	5853	140538	1.00	3	α Ser	5854	140573	1.28	1		5864	140901	0.96	2
λ Ser	5868	141004	1.05	1	ϵ Ser	5892	141795	1.81	1	β Tra	5897	141891	1.61	1
39 Ser	5911	142267	0.89	2	χ Her	5914	142373	0.98	1	γ Ser	5933	142860	1.16	1
θ Dra	5986	144284	1.63	2			144287	0.90	2	14 Her		145675	1.11	1
		145825	1.04	2	49 Ser		145958	0.89	2	18 Sco	6060	146233	0.99	1
σ CrB	6063	146361	1.14	5		6094	147513	1.06	2	ζ Tra	6098	147584	1.09	2
		149612	0.88	1			149806	0.98	2	ζ Her	6212	150680	1.40	2
ϵ Sco	6241	151680	1.24	1			152391	0.88	1	19 Dra	6315	153597	1.15	2
		154088	1.07	1			154345	0.97	1		6349	154417	1.10	1
η Oph	6378	155125	2.40	2	η Sco	6380	155203	1.92	1	δ Her	6410	156164	2.10	2
ξ Oph	6445	156897	1.30	2		6465	157347	0.96	3		6516	158614	0.98	2
	6538	159222	1.12	1	Rasalhague	6556	159561	2.18	2	λ Ara	6569	160032	1.22	2
26 Dra	6573	160269	1.08	3	μ Ara	6585	160691	1.13	1	58 Oph	6595	160915	1.20	1
ω Dra	6596	160922	1.38	2	μ Her	6623	161797	1.15	4	ψ^1 Dra	6636	162003	1.46	3
ζ Ser	6710	164259	1.48	1			164922	0.94	1		6748	165185	1.06	2
70 Oph	6752	165341	0.92	2	ι Pav	6761	165499	1.03	2	99 Her	6775	165908	1.00	2
		166435	1.05	1		6828	167425	1.13	2		6847	168009	1.00	1
36 Dra	6850	168151	1.18	2	η Ser	6869	168723	1.45	1	λ Sgr	6913	169916	1.13	1
χ Dra	6927	170153	1.04	2		6998	172051	0.90	1	Vega	7001	172167	2.30	1
110 Her	7061	173667	1.47	1		7162	176051	1.04	2			176377	0.97	1
γ CrA	7226	177474	1.15	2		7232	177565	0.96	1		7260	178428	1.04	2
	7294	179958	0.98	2			180161	1.01	1		7330	181321	1.01	2
	7368	182488	1.05	2	31 Aql	7373	182572	1.18	1	δ Aql	7377	182640	1.65	2
		184385	0.99	1	θ Cyg	7469	185395	1.40	4			185414	0.98	3
16 Cyg	7503	186408	1.03	3	17 Cyg	7534	187013	1.24	4	Altair	7557	187642	1.75	1
o Aql	7560	187691	1.21	2	β Aql	7602	188512	1.37	3		7631	189245	1.22	1
	7637	189340	1.08	2		7644	189567	0.93	1			190067	0.84	2
δ Pav	7665	190248	1.12	1		7670	190360	1.06	2	15 Sge	7672	190406	1.06	2
	7674	190422	1.14	1		7683	190771	1.13	2	27 Cyg	7689	191026	1.35	1
	7783	193664	0.99	1			194640	0.90	1		7845	195564	1.09	2
ϕ^2 Pav	7875	196378	1.17	1		7898	196761	0.87	1		7914	197076	0.98	3
η Ind	7920	197157	1.58	1			197214	0.88	3	ψ Cap	7936	197692	1.38	1
ϵ Cyg	7949	197989	1.61	3	η Cep	7957	198149	1.38	1		8013	199260	1.12	1
		199509	0.91	2		8061	200525	1.15	3	δ Equ	8123	202275	1.19	2
τ Cyg	8130	202444	1.65	4			202628	1.00	1		8148	202940	0.85	3
		203244	0.94	2	Alderamin	8162	203280	1.92	1	γ Pav	8181	203608	0.95	1
ν Oct	8254	205478	1.61	2			205536	0.89	1	μ^1 Cyg	8309	206826	1.35	2
	8314	206860	1.02	2	δ Cap	8322	207098	1.50	2		8323	207129	1.02	1
ι Peg	8430	210027	1.33	2			210277	1.07	1	τ PsA	8447	210302	1.28	1
		210667	1.00	1		8477	210918	0.97	1		8501	211415	0.97	2
	8526	212168	1.05	4		8531	212330	1.06	3	53 Aqr	8545	212698	1.06	3
υ Aqr	8592	213845	1.35	2		8635	214953	1.13	3	ξ Peg	8665	215648	1.17	2
Fomalhaut	8728	216956	1.89	3	51 Peg	8729	217014	1.11	1		8734	217107	1.11	1
		217813	1.09	1			218687	1.00	3			218868	1.08	2
7 And	8830	219080	1.56	1		8843	219482	1.16	1	γ Tuc	8848	219571	1.59	2
	8853	219623	1.14	1	94 Aqr	8866	219834	1.29	3			220182	0.85	1
	8964	222143	1.08	1	ι Psc	8969	222368	1.17	1	γ Cep	8974	222404	1.47	3
		224465	1.01	2										

expectation of many future revisions, however, we consider the general decrease (increase) of single (non-single) stars as a function of primary mass displayed in Figure 12 a very solid result.

As we have discussed in P1 and P2, on the high-mass side of Figure 12 the survey is lost in low-number bins and the uncertainties that arise from stellar rotation. On the low-mass side, the final set of stars included in Section 3 of this work

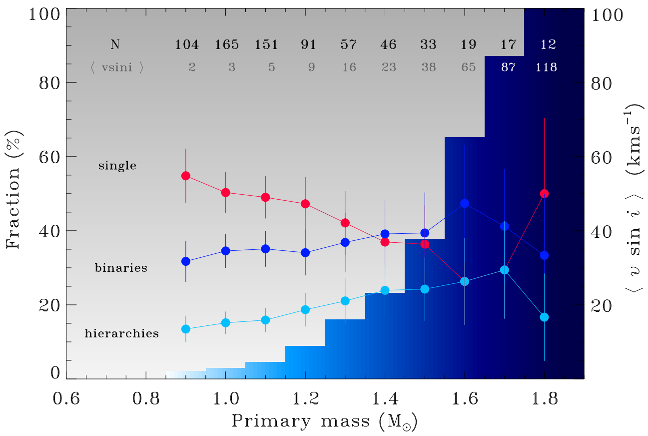

Figure 12. Multiplicities of the survey Population I stars as a function of their primary masses. The percentages of single, binary, and higher level systems are presented as a running mean of bin width 0.20 $M_\odot$ with the number of stars per bin as indicated in the legend. Average projected rotational velocities $\langle v \sin i \rangle$ are depicted with the blue shading. Except for the highest mass bins—which are mostly subject to Poisson noise (denoted by error bars) and high rotational velocities—there is a steady decline of the single-star fraction as a function of mass.

provides an important contribution, but it is clear from the relative numbers in Table 6 that the survey cannot be complete in both the 0.80–0.89 $M_\odot$ and 0.90–0.99 $M_\odot$ mass bins. This has to do with the main-sequence $T_{\rm eff} = 5300$ K cutoff effective temperature, which corresponds to masses of 0.70 $M_\odot$ to 1.10 $M_\odot$ for metal-poor and metal-rich stars, respectively.

There are three K-type stars with masses in the 1.00–1.09 $M_\odot$ mass bin, but they are not included in Figure 12 because of their low effective temperatures $T_{\rm eff} < 5300$ K. These are the triple systems HD 139341/23 and HD 203985, and the single star HD 13579. HD 139341/23 is the most metal-rich of them at [Fe/H] = +0.44, followed by HD 203985 at [Fe/H] = +0.36, and HD 13579 at [Fe/H] = +0.34.

In the 0.90–0.99 $M_\odot$ mass bin are located 11 metal-rich K dwarfs[11] with $+0.00 \leqslant$ [Fe/H] $\leqslant +0.33$ and $T_{\rm eff} < 5300$ K, but as the bin number in Table 6 also implies, at least some 20 or 30 more metal-poor stars must also be lacking in this mass bin. Therefore, and in terms of the primary masses, we can conclude that starting with the 1.00–1.10 $M_\odot$ mass bin, the survey is essentially complete, whereas in the 0.90–0.99 $M_\odot$ mass bin a considerable fraction of stars is lacking, and hence the points in the leftmost bin in Figure 12 are less representative.

In the final two columns of Table 6 we restrict the census to stars in the mass range $0.90 \leqslant M \leqslant 1.70\, M_\odot$, i.e., approximately to all F- and G-type stars. Here, the comparison of the all-sky survey with the northern sample confirms the previously found imbalance of the stellar multiplicities, with the southern hemisphere being the much less explored (cf. Chini et al. 2014). With respect to the more complete northern sample of F- and G-type stars in the final column of Table 6, our census results in 57.6% non-single stars and 21.0% higher level systems. We note that by inclusion of the massive ($M \geqslant 0.90\, M_\odot$) but cool ($T_{\rm eff} < 5300$ K) metal-rich K dwarfs discussed above, these numbers would change to 58.4% non-single stars and 21.3% higher level systems.

4.2. Population II and Intermediate-disk Stars

For the old stars of the Galaxy we cannot provide a similar diagram as Figure 12, the reason being that except for blue stragglers, the stars above approximately one solar mass have all turned into stellar remnants, as we can infer from Table 7. This also applies to the somewhat younger intermediate-disk stars that are set out in Table 8. For the latter, and contrary to the census in Raghavan et al. (2010), we agree with Heintz (1986) in considering HD 135204 a doubtful case for a binary. In particular, a close system with equal components, as repeatedly stated for HD 135204 in the literature, immediately leads to implausible positions below the main sequence. For ρ CrB, in turn, we follow Reffert & Quirrenbach (2011), who find its companion to be of stellar mass, although this result is not without more recent dispute in Fulton et al. (2016). For the Population II stars, advances in comparison to the multiplicities in Raghavan et al. (2010) include HD 18757 (Bouchy et al. 2016), HD 165401 (Chini et al. 2014), and 85 Peg (Jefferies & Christou 1993; Griffin 2004), which are all triple systems, whereas HD 68017 is now a confirmed binary (Crepp et al. 2012).[12] Furthermore, two F-type blue straggler stars, HR 3220 and HR 4657, were not included in Raghavan et al. (2010) because of their too blue colors, and finally, the evidence for HD 159062 to harbor a white dwarf companion will be discussed in a forthcoming contribution (K. Fuhrmann et al. 2017, in preparation).

While the small numbers of Population II ($N = 22$) and intermediate-disk stars ($N = 9$) in Tables 7 and 8 certainly cannot provide a solid basis for their multiplicities, some provisional findings appear worthwhile to report, however. To this end, we group in Figure 13 the two subsets of old-disk stars together and compare their relative fractions of single, binaries, and multiples to the 104 Population I stars with subsolar masses of Table 6. Interestingly, the old-disk stars display higher multiplicities throughout, and we may conjecture that this may be due to their somewhat different metallicities. However, this is not observed for the metal-rich and metal-poor Population I stars (cf. Fuhrmann 2011, Figure 17), which in turn considerably overlap in abundance with the Population II and intermediate-disk stars. It would then appear more likely that the higher multiplicities of the old stars, if confirmed, reflect the star formation products in a violent environment, as was very likely the case of the early Milky Way. We stress again that in Figure 13 we can only refer to a small set of 31 ancient sources, but with an average stellar mass $\langle M \rangle = 0.88\, M_\odot$ it is quite remarkable that only 11 of them appear to be single. Comparative multiplicities for the Population I stars in Figure 12 are not achieved before $\langle M \rangle = 1.40\, M_\odot$.

Provided that star formation in starburst environments leads to higher stellar multiplicities, this would mean that dynamical interactions in the early star clusters and orbital evolution at later stages must be comparatively more important. If at least two-thirds of the ancient G-type stars are indeed non-single, and given their long timescale of evolution, it is perhaps no surprise to find a significant fraction of mass-transfer systems, blue straggler stars, and white dwarf companions, as we have

[11] These are 54 Psc, HD 17382, HD 18143, HD 21175, HR 1925, HD 52698, HD 72760, HR 5553, 12 Oph, HD 200968, and HD 221354.

[12] With reference to the very recent *Gaia* DR1 release, we note that HR 3578, a likely spectroscopic binary previously reported in Nordström et al. (2004), now also displays a *Hipparcos/Gaia* discrepancy (DQ) value of the same magnitude as the Population II star HD 18757, where Bouchy et al. (2016) most recently found a brown dwarf companion; accordingly, we are inclined to count HR 3578 as a binary in Table 7.

Table 6
Multiplicities of the Survey Population I Stars

	0.80–0.89 ($M_\odot$)	0.90–0.99 ($M_\odot$)	1.00–1.09 ($M_\odot$)	1.10–1.19 ($M_\odot$)	1.20–1.29 ($M_\odot$)	1.30–1.39 ($M_\odot$)	1.40–1.49 ($M_\odot$)	1.50–1.59 ($M_\odot$)	1.60–1.69 ($M_\odot$)	1.70–1.79 ($M_\odot$)	1.80–1.89 ($M_\odot$)	1.90+ ($M_\odot$)	Σ All-sky	F+G All-sky	F+G North
All	33	71	94	57	34	23	23	10	9	8	4	25	391	323	210
Single	20	37	46	28	15	9	8	4	1	4	2	10	184	148	89
	(60.6)	(52.1)	(48.9)	(49.1)	(44.1)	(39.1)	(34.8)	(40.0)	(11.1)	(50.0)	(50.0)	(40.0)	(47.1)	(45.8)	(42.4)
Binaries	9	24	33	20	11	10	8	5	4	3	1	8	136	116	77
	(27.3)	(33.8)	(35.1)	(35.1)	(32.4	(43.5)	(34.8)	(50.0)	(44.4)	(37.5)	(25.0)	(32.0)	(34.8)	(35.9)	(36.7)
Hierarchies	4	10	15	9	8	4	7	1	4	1	1	7	71	59	44
	(12.1)	(14.1)	(16.0)	(15.8)	(23.5)	(17.4)	(30.4)	(10.0)	(44.4)	(12.5)	(25.0)	(28.0)	(18.2)	(18.3)	(21.0)
$\langle v \sin i \rangle$	1.8	2.3	3.4	6.4	13.0	20.5	25.7	65.3	65.0	111.9	128.8	122.2	$\cdots$	$\cdots$	$\cdots$

Note. Relative percentages of single, binary, and higher level systems are given in parentheses. Average projected rotational velocities $\langle v \sin i \rangle$ in the final row are in units of km s^{-1}. The last two columns refer to the stars in the mass range $0.90 \leqslant M \leqslant 1.70\ M_\odot$—denoted as F- and G-type stars—either all-sky or north of $\delta = -15°$. Note here the imbalance of the stellar multiplicities, which is direct evidence of an as yet less explored southern hemisphere. With respect to the most significant northern sample of F- and G-type stars in the final column, this census provides 21% in hierarchies, and 58% are non-single.

Table 7
Multiplicity Census of the Survey Population II Stars

Object	HR	HD	Mass ($M_\odot$)	N	Object	HR	HD	Mass ($M_\odot$)	N	Object	HR	HD	Mass ($M_\odot$)	N
	⋯	4308	0.92	1	μ Cas	321	6582	0.73	2	τ Cet	509	10700	0.78	1
	⋯	18757	0.90	3	82 Eri	1008	20794	0.85	1	⋯	3018	63077	0.86	3
	⋯	64606	0.70	2	⋯	⋯	65583	0.73	1	⋯	3138	65907	1.03	3
	⋯	68017	0.84	2	⋯	3220	68456	1.35	2	⋯	3578	76932	0.86	2
	4657	106516	0.90	2	Arcturus	5340	124897	0.59	1	ν^2 Lup	5699	136352	0.92	1
	⋯	144579	0.74	2	72 Her	6458	157214	0.91	1	⋯	⋯	159062	0.83	2
	⋯	165401	0.93	3	⋯	⋯	195987	0.84	2	⋯	⋯	199288	0.85	1
85 Peg	9088	224930	0.76	3	⋯	⋯	⋯	⋯	⋯	⋯	⋯	⋯	⋯	⋯

Table 8
Multiplicity Census of the Survey Intermediate-disk Stars

Object	HR	HD	Mass ($M_\odot$)	N	Object	HR	HD	Mass ($M_\odot$)	N	Object	HR	HD	Mass ($M_\odot$)	N
104 Tau	1656	32923	0.98	1	⋯	⋯	40397	0.89	3	⋯	2667	53705	0.98	4
	4098	90508	0.94	2	⋯	⋯	97343	0.89	1	⋯	4523	102365	0.90	2
	5566	131923	0.99	2	⋯	⋯	135204	0.85	1	ρ CrB	5968	143761	0.97	2

Table 9
Multiplicity Census of the Survey Population I Stars and Evolution Within the Last Decade

	Northern Sample (2007 Jun)		Northern Sample (2010 Oct)		Northern Sample (2016 Jul)		Southern Sample (2016 Jul)		All-sky Survey (2016 Jul)	
	N	(%)	N	(%)	N	(%)	N	(%)	N	(%)
Star systems	255		254		252		139		391	
Single stars	126	49.4	118	46.5	113	44.8	71	51.1	184	47.1
Binary systems	93	36.5	97	38.2	89	35.3	47	33.8	136	34.8
Triple systems	24	9.4	26	10.2	35	13.9	17	12.2	52	13.3
Quadruple systems	9	3.5	9	3.5	11	4.4	4	2.9	15	3.8
Higher level systems	3	1.2	4	1.6	4	1.6	⋯	⋯	4	1.0
Multiplicity level	⋯	71.0	⋯	76.0	⋯	82.9	⋯	66.9	⋯	77.2

Note. Note the progressive shift toward non-single stars and higher level systems for the northern sample. The comparison of the multiplicity levels, defined as the number of companions per primary star, shows that the progress for the southern sample is delayed by more than a decade with respect to the northern sample.

pointed out in P3. Nearby single key subgiants, like 104 Tau, among these stars consistently suggest that they are extremely old (Bernkopf & Fuhrmann 2006), but many others like HR 4657 (Fuhrmann & Bernkopf 1999), HR 3220 (Fuhrmann et al. 2011c), or HR 3138 (Fuhrmann et al. 2012), taken at face value, will purport much younger, and hence incorrect, stellar ages.

5. Discussion

Two decades ago, the *Hipparcos* experiment established the local inventory of the F- and G-type stars within 25 pc. In terms of their stellar companions, and in spite of the technological progress since then, we are still far from a complete census, however. Some of the obstacles involved ironically have to do with the nearness of the targets. Many of the stars are simply too bright for deep all-sky surveys, and second, potential companions can have angular distances of tens of arcminutes up to degrees, the southern triple α Cen being the classical example. Moreover, many early observations did or could only report the discovery of common-proper-motion visual companions, without a closer follow-up of the mostly faint secondaries. Decades and even centuries later, high spatially resolved direct imaging and high-resolution spectroscopy now start to demonstrate that a significant fraction of these companions are themselves part of close subsystems. The tertiary component of HR 8635 reported above in this work, for instance, was first disclosed in 2015 December through high-resolution spectroscopy (cf. Figure 11). The M-dwarf visual companion in contrast has been known since the late nineteenth century.

As a result of these recent discoveries, the focus of our understanding of star formation progressively shifts from the classical textbook binary with an ordinary mostly well-understood evolution to more sophisticated hierarchical systems with principally much more complex evolutionary and orbital paths.

The progress that has taken place in the past decade on the stellar multiplicities of the Population I stars for the northern sample can be traced in Table 9. The most remarkable point is the rapid evolution among the triple and higher level systems with, currently, a 20% fraction. At the same time, the single stars have become a minority and will likely continue to do so. It is possible that this may only end with the one-third percentage originally assessed by Duquennoy & Mayor (1991). Table 9 also demonstrates that south of $\delta = -15°$ our

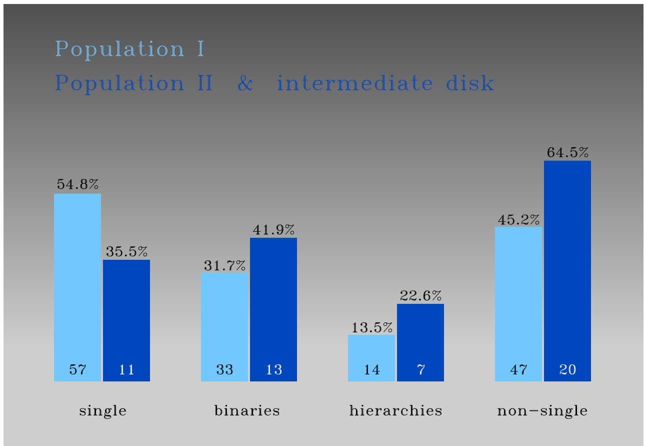

Figure 13. Multiplicities of the survey Population II and intermediate-disk stars ($N = 31$, dark blue) compared to the subsolar mass Population I stars ($N = 104$, light blue) of Table 6. Percentages and number of stars per multiplicity bin are given. There is evidence of a higher fraction of binaries and multiple systems in the early Milky Way (see text for details).

knowledge of the stellar multiplicities is even more incomplete. To reach the level of the single stars of the northern sample, for instance, 9 of the 71 southern single stars would need to have a companion. The comparison of the multiplicity levels in the final row, defined as the number of companions per primary star, shows that the progress for the southern stars is currently more than a decade behind that of the northern sample.

Although the survey can only refer to 22 Population II and 9 intermediate-disk stars, it appears that the early epoch of the Galaxy was characterized by an even larger fraction of binary stars and higher level systems. For the Population II and intermediate-disk stars with average masses of $\langle M \rangle = 0.86\, M_\odot$ and $\langle M \rangle = 0.93\, M_\odot$, respectively, we find that at least two out of three sources are non-single, and the fraction of higher level systems exceeds 20%. If confirmed with larger samples, this would be a remarkable finding, as these multiplicity levels are by no means reached for the Population I stars of comparable mass. The multiplicities suggest that as a Population II star, the Sun would likely not be without a companion.

In this context, it is an important result that the major fraction of the survey Population II stars (HR 3018, HR 3138, HR 3220, HR 4657, HD 159062, and HD 165401) are either mass-transfer systems or possess a white dwarf companion, since it shows that conventional stellar age datings will not succeed if the previous evolution of these systems remains in the dark. For the nearby stars, many with a long record of observations, there is necessarily a higher success rate, although Arcturus, the very nearby and brightest of the local Population II stars, may rather serve as a good counter-example. The results for the local Population II stars immediately raise the question, however, how efficient we can be with distant surveys of ancient stars if the bulk of them is indeed not single and a greater portion of them need to be considered to consist of blue straggler stars.

In Section 2 above, we have mentioned the Population I visual binary γ Vir ($P = 169$ years), a prominent and usually well-separable system. For the past two decades, γ Vir was close to its periastron passage and only allowed us to secure a composite unresolved spectrum (cf. Figure 1). Although this situation does currently improve because of its nearness, at a distance of just 50 pc γ Vir would remain an adaptive optics target at any orbital phase, and at kiloparsec distances it would not be resolvable at all. While γ Vir was already discovered as a visual binary with modest observational equipment almost 300 years ago, as a distant object its radial velocity cross-correlation function therefore would—unlike in Figure 1—not show any asymmetry for many decades. Without realizing that it is a twin system, straight consequences would be an incorrect distance and hence incorrect kinematics.

With these examples for young- and old-disk stars, the conclusion is that a good understanding of distant surveys can only succeed if we know what is locally relevant. The fact that two-thirds of the local F-type stars have a known companion, but only one-third are known in the case of the local degenerates provides not much confidence for distant and local surveys.

This work has made extensive use of the *Catalog of Nearby Stars* (CNS4) of the Astronomisches Rechen-Institut at Heidelberg, Germany, the ESA *Hipparcos* catalog, NASA's ADS bibliographic service, and the CDS *SIMBAD* database, operated at Strasbourg, France. Based on observations collected at the Centro Astronómico Hispano Alemán (CAHA) at Calar Alto, operated jointly by the Max-Planck Institut für Astronomie and the Instituto de Astrofísica de Andalucía (CSIC). Based on observations in Chile at the Universitäts-sternwarte Bochum near Cerro Armazones and the La Silla Paranal Observatory under ESO programmes ID 092.A-9002 (A) and 096.A-9009(A). K.F. acknowledges support from the DFG grants FU 198/10-1 and 10-2. Z.C. thanks for the support by NSFC 11503087 and the Sino-German (CSC-DAAD) Postdoc Scholarship Program. We are grateful to R. Angeloni, A. Hempel, R. Lachaume, and M. Rabus for their support with the FEROS observations in La Silla, and to our colleagues A. Barr, L.-S. Buda, T. Dembsky, H. Drass, M. Hackstein, R. Lemke, F. Pozo Nuñez, M. Ramolla, and C. Westhues for their help with BESO. This publication is supported as a project of the Nordrhein-Westfälische Akademie der Wissenschaften und der Künste in the framework of the academy program by the Federal Republic of Germany and the state Nordrhein-Westfalen.

References

Abt, H. A., & Levy, S. G. 1976, ApJS, 30, 273
Abt, H. A., & Willmarth, D. 2006, ApJS, 162, 207
Alden, H. L. 1936, AJ, 45, 73
Alonso, A., Arribas, S., & Martínez-Roger, C. 1995, A&A, 297, 197
Andersen, J., & Nordström, B. 1983, A&A, 122, 23
Bergbusch, P. A., & Stetson, P. B. 2009, AJ, 138, 1455
Bernkopf, J., & Fuhrmann, K. 2006, MNRAS, 369, 673
Bopp, B. W., Evans, D. S., & Laing, J. D. 1970, MNRAS, 147, 355
Borgniet, S., Lagrange, A.-M., Meunier, N., & Galland, F. 2016, A&A, in press (arXiv:1608.08257)
Bouchy, F., Ségransan, D., Díaz, R. F., et al. 2016, A&A, 585, A46
Bowyer, S., Lieu, R., Lampton, M., et al. 1994, ApJS, 93, 569
Bromage, G. E., Buckley, D. A. H., Gilmore, A. C., et al. 1996, IBVS, 4400, 1
Caballero, J. A., & Montes, D. 2012, Obs, 132, 176
Carretta, E., Gratton, R. G., Clementini, G., & Fusi Pecci, F. 2000, ApJ, 533, 215
Catchpole, R. M. 1972, Obs, 92, 125
Chaboyer, B., Demarque, P., Kernan, P. J., & Krauss, L. M. 1998, ApJ, 494, 96
Chini, R., Fuhrmann, K., Barr, A., et al. 2014, MNRAS, 437, 879
Chini, R., Fuhrmann, K., Pozo Nuñez, F., et al. 2016, AN, 337, 621
Crepp, J. R., Johnson, J. A., Howard, A. W., et al. 2012, ApJ, 761, 39
Cutispoto, G., Kürster, M., Messina, S., et al. 1997, A&A, 320, 586
Cutispoto, G., Pallavicini, R., Kürster, M., & Rodonò, M. 1995, A&A, 297, 764

Dawson, B. H. 1933, AJ, 43, 15
Donner, H. F. 1953, AJ, 58, 164
Duquennoy, A., & Mayor, M. 1991, A&A, 248, 485
Eggen, O. J. 1952, PASP, 64, 230
Eggen, O. J. 1960, MNRAS, 120, 540
Eggen, O. J. 1986, AJ, 92, 910
Eggen, O. J. 1996, AJ, 111, 1615
Ehrenreich, D., Lagrange, A.-M., Montagnier, G., et al. 2010, A&A, 523, A73
Endl, M., Brugamyer, E. J., Cochran, W. D., et al. 2016, ApJ, 818, 34
Ferrario, L. 2012, MNRAS, 426, 2500
Fuhrmann, K. 2000, http://www.ing.iac.es/~klaus/
Fuhrmann, K. 2004, AN, 325, 3
Fuhrmann, K. 2011, MNRAS, 414, 2893
Fuhrmann, K., & Bernkopf, J. 1999, A&A, 347, 897
Fuhrmann, K., & Chini, R. 2012, ApJS, 203, 30 (P1)
Fuhrmann, K., & Chini, R. 2015a, ApJ, 806, 163
Fuhrmann, K., & Chini, R. 2015b, ApJ, 809, 107 (P2)
Fuhrmann, K., Chini, R., Buda, L.-S., & Pozo Nuñez, F. 2014, ApJ, 785, 68
Fuhrmann, K., Chini, R., Haas, M., et al. 2012, ApJ, 761, 159
Fuhrmann, K., Chini, R., Hoffmeister, V. H., et al. 2011a, MNRAS, 411, 2311
Fuhrmann, K., Chini, R., Hoffmeister, V. H., & Stahl, O. 2011b, MNRAS, 415, 1240
Fuhrmann, K., Chini, R., Hoffmeister, V. H., & Stahl, O. 2011c, MNRAS, 416, 391
Fuhrmann, K., Chini, R., Kaderhandt, L., et al. 2016, MNRAS, 459, 1682
Fuhrmann, K., Chini, R., Kaderhandt, L., & Chen, Z. 2017, MNRAS, 464, 2610 (P3)
Fuhrmann, K., Pfeiffer, M., Frank, C., et al. 1997, A&A, 323, 909
Fulton, B. J., Howard, A. W., Weiss, L. M., et al. 2016, ApJ, 830, 46
Gliese, W. 1957, MiARI, 8, 1
Goldin, A., & Makarov, V. V. 2006, ApJS, 166, 341
Gray, D. F. 1984, ApJ, 281, 719
Gray, D. F. 1992, The Observation and Analysis of Stellar Photospheres (Cambridge: Cambridge Univ. Press)
Griffin, R. F. 2001, Obs, 121, 221
Griffin, R. F. 2004, Obs, 124, 258
Grundahl, F., Stetson, P. B., & Andersen, M. I. 2002, A&A, 395, 481
Gullikson, K., Endl, M., Cochran, W. D., & MacQueen, P. J. 2015, ApJ, 815, 62
Haas, J. 1930, AN, 239, 97
Hale, A. 1994, AJ, 107, 306
Hartkopf, W. I., & Mason, B. D. 2010, IAUDS, 170, 2
Heintz, W. D. 1978, ApJS, 37, 515
Heintz, W. D. 1986, AJ, 92, 446
Holberg, J. B., Oswalt, T. D., Sion, E. M., et al. 2013, MNRAS, 435, 2077
Hünsch, M., Schmitt, J. H. M. M., Sterzik, M. F., & Voges, W. 1999, A&AS, 135, 319
Iben, I., Jr., & Tutukov, A. V. 1999, ApJ, 511, 324
Jancart, S., Jorissen, A., Babusiaux, C., & Pourbaix, D. 2005, A&A, 442, 365
Janson, M., Hormuth, F., Bergfors, C., et al. 2012, ApJ, 754, 44
Jasinta, D. M. D. 1997, in Visual Double Stars: Formation, Dynamics and Evolutionary Tracks, ed. J. A. Docobo, A. Elipe, & H. McAlister (Dordrecht: Kluwer), 367
Jefferies, S. M., & Christou, J. C. 1993, ApJ, 415, 862
Jenkins, J. S., Díaz, M., Jones, H. R. A., et al. 2015, MNRAS, 453, 1439
Jenkins, J. S., Jones, H. R. A., Biller, B., et al. 2010, A&A, 515, A17
Jódar, E., Pérez-Garrido, A., Díaz-Sánchez, A., et al. 2013, MNRAS, 429, 859
Jones, H. R. A., Butler, R. P., Tinney, C. G., et al. 2002, MNRAS, 333, 871
Katz, B., Dong, S., & Kushnir, D. 2014, arXiv:1402.7083
Kaufer, A., Stahl, O., Tubbesing, S., et al. 1999, Msngr, 95, 8
Kroupa, P. 2002, MNRAS, 330, 707
Makarov, V. V., Zacharias, N., & Hennessy, G. S. 2008, ApJ, 687, 566
Mohr, J. M. 1930, BuAst, 6, 147
Naef, D., Mayor, M., Pepe, F., et al. 2001, A&A, 375, 205
Nidever, D. L., Marcy, G. W., Butler, R. P., et al. 2002, ApJS, 141, 503
Nordström, B., Mayor, M., Andersen, J., et al. 2004, A&A, 418, 989
Pasquini, L., Liu, Q., & Pallavicini, R. 1994, A&A, 287, 191
Pepe, F., Lovis, C., Ségransan, D., et al. 2011, A&A, 534, A58
Percival, S. M., Salaris, M., van Wyk, F., & Kilkenny, D. 2002, ApJ, 573, 174
Perryman, M. A. C., Lindegren, L., Kovalevsky, J., et al. 1997, A&A, 323, L49
Pfeiffer, M. J., Frank, C., Baumüller, D., et al. 1998, A&AS, 130, 381
Potter, D., Martín, E. L., Cushing, M. C., et al. 2002, ApJL, 567, L133
Pounds, K. A., Allan, D. J., Barber, C., et al. 1993, MNRAS, 260, 77
Pravdo, S. H., Shaklan, S. B., Wiktorowicz, S. J., et al. 2006, ApJ, 649, 389
Raghavan, D., McAlister, H. A., Henry, T. J., et al. 2010, ApJS, 190, 1
Rappaport, S., Podsiadlowski, Ph., Joss, P. C., et al. 1995, MNRAS, 273, 731
Reffert, S., & Quirrenbach, A. 2011, A&A, 527, A140
Riddle, R. L., Tokovinin, A., Mason, B. D., et al. 2015, ApJ, 799, 4
Rodriguez, D. R., Duchêne, G., Tom, H., et al. 2015, MNRAS, 449, 3160
Sahlmann, J., Ségransan, D., Queloz, D., et al. 2011, A&A, 525, A95
Scardia, M., Argyle, R. W., Prieur, J.-L., et al. 2007, AN, 328, 146
Scardia, M., & Pansecchi, L. 2005, IAUDS, 156, 1
Shaya, E. J., & Olling, R. P. 2011, ApJS, 192, 2
Söderhjelm, S. 1999, A&A, 341, 121
Steffen, M. 1985, A&AS, 59, 403
Steiner, I., Seifert, W., Stahl, O., et al. 2006, Proc. SPIE, 6269, 2
Tagliaferri, G., Covino, S., Cutispoto, G., & Pallavicini, R. 1999, A&A, 345, 514
Tokovinin, A. 2012, AJ, 144, 56
Tokovinin, A. 2013, AJ, 145, 76
Tokovinin, A. 2014a, AJ, 147, 86
Tokovinin, A. 2014b, AJ, 147, 87
Tokovinin, A., Mason, B. D., & Hartkopf, W. I. 2010, AJ, 139, 743
Tokovinin, A., Mason, B. D., & Hartkopf, W. I. 2014, AJ, 147, 123
Tokovinin, A., Mason, B. D., Hartkopf, W. I., et al. 2015a, AJ, 150, 50
Tokovinin, A., Pribulla, T., & Fischer, D. 2015b, AJ, 149, 8
Tokovinin, A., Thomas, S., Sterzik, M., & Udry, S. 2006, A&A, 450, 681
Toyota, E., Itoh, Y., Ishiguma, S., et al. 2009, PASJ, 61, 19
van Leeuwen, F. 2007, A&A, 474, 653
VandenBerg, D. A., Bergbusch, P. A., & Dowler, P. D. 2006, ApJS, 162, 375
VandenBerg, D. A., Casagrande, L., & Stetson, P. B. 2010, AJ, 140, 1020
Watson, L. C., Pritchard, J. D., Hearnshaw, J. B., et al. 2001, MNRAS, 325, 143
Willmarth, D. W., Fekel, F. C., Abt, H. A., & Pourbaix, D. 2016, ApJ, 152, 46
Wittenmyer, R. A., Butler, R. P., Tinney, C. G., et al. 2016, ApJ, 819, 28
Wittenmyer, R. A., Tinney, C. G., O'Toole, S. J., et al. 2011, ApJ, 727, 102
Zirm, H. 2014, IAUDS, 182, 2
Zuckerman, B., Vican, L., Song, I., & Schneider, A. 2013, ApJ, 778, 5